Please cite this article in press as: Saupe et al., Tenascin-C Downregulates Wnt Inhibitor Dickkopf-1, Promoting Tumorigenesis in a Neuroendocrine Tumor Model, Cell Reports (2013), http://dx.doi.org/10.1016/j.celrep.2013.09.014

Cell Reports
Article

Tenascin-C Downregulates Wnt Inhibitor Dickkopf-1, Promoting Tumorigenesis in a Neuroendocrine Tumor Model

Falk Saupe,[1,2,3,4,12] Anja Schwenzer,[1,2,3,4,12] Yundan Jia,[1,2,3,4,5,12] Isabelle Gasser,[1,2,3,4] Caroline Spenlé,[1,2,3,4] Benoit Langlois,[1,2,3,4] Martial Kammerer,[1,2,3,4] Olivier Lefebvre,[1,2,3,4] Ruslan Hlushchuk,[6] Tristan Rupp,[1,2,3,4] Marija Marko,[1,2,3,4] Michael van der Heyden,[1,2,3,4] Gérard Cremel,[1,2,3,4] Christiane Arnold,[1,2,3,4] Annick Klein,[1,2,3,4] Patricia Simon-Assmann,[1,2,3,4] Valentin Djonov,[6] Agnès Neuville-Méchine,[7] Irene Esposito,[8] Julia Slotta-Huspenina,[8] Klaus-Peter Janssen,[9] Olivier de Wever,[10] Gerhard Christofori,[11] Thomas Hussenet,[1,2,3,4,*] and Gertraud Orend[1,2,3,4,5,*]

[1]Inserm U1109, MN3T Team, The Microenvironmental Niche in Tumorigenesis and Targeted Therapy, 3 Avenue Molière, 67200 Strasbourg, France

[2]Université de Strasbourg, 67000 Strasbourg, France

[3]LabEx Medalis, Université de Strasbourg, 67000 Strasbourg, France

[4]Fédération de Médecine Translationnelle de Strasbourg (FMTS), 67000 Strasbourg, France

[5]Institute of Biochemistry and Genetics, Department of Biomedicine, University of Basel, Extracellular Matrix Adhesion Team, Mattenstraße 28, 4058 Basel, Switzerland

[6]Institute of Anatomy, University of Bern, Baltzerstrasse 2, 3000 Bern, Switzerland

[7]Hospital Hautepierre, Department of Anatomy and Pathology, 1 Avenue Molière, 67200 Strasbourg, France

[8]Institute of Pathology and Anatomy, Technical University Munich, Trogerstrasse 18, 81675 München, Germany

[9]Department of Surgery Technical University Munich, Ismaningerstrasse 22, 81675 München, Germany

[10]Laboratory of Experimental Cancer Research, Department of Radiation Oncology and Experimental Cancer Research, Ghent University Hospital, De Pintelaan 185, 9000 Ghent, Belgium

[11]Institute of Biochemistry and Genetics, Department of Biomedicine, University of Basel, Switzerland, Tumor Biology Team, Mattenstraße 28, 4058 Basel, Switzerland

[12]These authors contributed equally to this work

*Correspondence: hussenetthomas@gmail.com (T.H.), gertraud.orend@inserm.fr (G.O.)

http://dx.doi.org/10.1016/j.celrep.2013.09.014

SUMMARY

The extracellular matrix molecule tenascin-C (TNC) is a major component of the cancer-specific matrix, and high TNC expression is linked to poor prognosis in several cancers. To provide a comprehensive understanding of TNC's functions in cancer, we established an immune-competent transgenic mouse model of pancreatic β-cell carcinogenesis with varying levels of TNC expression and compared stochastic neuroendocrine tumor formation in abundance or absence of TNC. We show that TNC promotes tumor cell survival, the angiogenic switch, more and leaky vessels, carcinoma progression, and lung micrometastasis. TNC downregulates Dickkopf-1 (*DKK1*) promoter activity through the blocking of actin stress fiber formation, activates Wnt signaling, and induces Wnt target genes in tumor and endothelial cells. Our results implicate DKK1 downregulation as an important mechanism underlying TNC-enhanced tumor progression through the provision of a proangiogenic tumor microenvironment.

INTRODUCTION

Manifestation of cancer requires many steps in which the microenvironment plays an essential role (Bissell and Labarge, 2005). A group of tumor cells with oncogenic mutations does not readily cause cancer, a phenomenon known as tumor dormancy (Aguirre-Ghiso, 2007). Angiogenesis presents an important step in awakening quiescent tumors and in driving their development into metastatic cancer (Almog, 2010). Tumor cells secrete soluble factors that attract endothelial cells (Kerbel, 2008). In addition, the extracellular matrix (ECM) constitutes a major fraction of cancer tissue and contributes to tumor angiogenesis and metastasis (Lu et al., 2012). An important component of the tumor-specific ECM is tenascin-C (TNC). TNC is known to promote malignant tumor progression and lung metastasis; yet, the underlying mechanisms are poorly understood (Midwood et al., 2011).

Because no stochastic and immune-competent in vivo model existed that would recapitulate the roles of TNC in tumor progression, we generated mouse lines with different expression levels of TNC (overexpression, wild-type, knockout) in the Rip1-Tag2 (RT2) model of pancreatic β-cell carcinogenesis (Hanahan, 1985). This model recapitulates multistage tumorigenesis as observed in most human cancers (Nevins, 2001; Pipas and Levine, 2001).

Please cite this article in press as: Saupe et al., Tenascin-C Downregulates Wnt Inhibitor Dickkopf-1, Promoting Tumorigenesis in a Neuroendocrine Tumor Model, Cell Reports (2013), http://dx.doi.org/10.1016/j.celrep.2013.09.014

Cell PRESS
Open ACCESS

Here, we demonstrate that TNC promotes several steps in RT2 tumorigenesis including the angiogenic switch and lung micrometastasis. We provide a mechanistic basis showing that TNC downregulates expression of the soluble Wnt inhibitor Dickkopf-1 (DKK1) (Glinka et al., 1998) by blocking actin stress fiber formation and induces canonical Wnt signaling in tumor and endothelial cells. Our data suggest that DKK1 downregulation by TNC in tumor and stromal cells may provide a tumorigenesis signaling promoting microenvironment. Given that Wnt signaling is a crucial pathway driving angiogenesis and is activated by TNC, this pathway may play an important role in promoting tumor angiogenesis and metastasis by TNC. Thus, targeting TNC or its associated signaling pathways may represent a strategy to counteract tumor progression.

RESULTS

Tenascin-C Promotes Tumor Cell Survival, Proliferation, and Invasiveness

To address whether TNC potentially plays a role in the RT2 model (Hanahan, 1985), we determined TNC expression during RT2 tumorigenesis by immunofluorescence microscopy analysis (immunofluorescence [IF]). In normal pancreatic islets, TNC expression was undetectable, whereas a large fraction of hyperplastic and almost all angiogenic and tumorigenic islets expressed TNC (Figure S1A), suggesting a potential role of TNC during RT2 tumor progression. Therefore, we generated RT2 mice with overexpression of TNC (RT2/TNC) and a lack of TNC (RT2/TNCKO) (Figures S1B–S1G).

We performed tissue analysis to address whether ectopically expressed TNC had an effect on cell proliferation. We quantified the proportion of cells positive for phosphohistone-H3 by IF (Figure S2A) and observed that tumors of RT2/TNC mice exhibited 1.4-fold more proliferating cells than those from RT2 mice (Figure 1A) with a significant difference in hyperplastic islets (Figure S2C). Surprisingly, a similar difference was also seen in RT2/TNCKO tumors (Figures 1B and S2D). We also investigated a potential impact of ectopically expressed TNC on apoptosis by staining for cleaved caspase-3 (Figure S2B). RT2/TNC tumors exhibited 2.8-fold less apoptotic cells than RT2 wild-type tumors (Figures 1C and S2E). In contrast, apoptosis was unchanged in RT2/TNCKO tumors in comparison to RT2 controls (Figures 1D and S2F). However, no difference was seen in tumor multiplicity or tumor volume between genotypes (Figures S2G and S2H). Interestingly, upon tumor grading we observed that the frequency of carcinomas and the ratio of carcinomas over adenomas were higher in RT2/TNC mice (1.8) than in RT2 controls (0.8) (Figure 1E; Table S1). We conclude that transgenic TNC increases proliferation and survival in RT2/TNC mice and more importantly promotes tumor progression.

Tenascin-C Promotes the Angiogenic Switch and the Formation of Leaky and Abnormal Tumor Vessels

To address whether TNC has an effect on RT2 tumor angiogenesis, we isolated islets at the age of 8 weeks when the angiogenic switch takes place in a subset of neoplastic islets (Hanahan et al., 1996; Parangi et al., 1996) (Figure S2I). We noticed that the number of angiogenic islets was 2.4-fold higher in RT2/TNC and 2.9-fold lower in RT2/TNCKO mice in comparison to RT2 littermates (Figures 1F and 1G; Table S2). By quantification of CD31-positive endothelial cells (Figure S2J) in tumor sections of 12-week-old RT2 mice, we observed that the abundance of blood vessels was 2.6-fold higher and 1.6-fold lower in tumors of RT2/TNC and RT2/TNCKO mice, respectively, than in RT2 controls (Figures 1H and 1I).

We next addressed the question of a potential impact of TNC on vessel anatomy by scanning electron microscopy in Mercox corrosion casts of the tumor vasculature of multiple tumors of RT2 and RT2/TNC mice. Using this descriptive approach, we observed a highly aberrant vessel phenotype in some RT2/TNC tumors that has not been seen in RT2 tumors. These vessels were irregularly shaped, wider, discontinued, and bifurcated (see arrows), reminiscent of high vessel branching and/or leakage (Figures 1J and S2K). Because this approach is not suitable for quantitative determinations, we then studied vessel lining by pericytes using NG2 staining as readout for vessel functionality and maturation (Figure S2L). Despite more abundant pericytes in RT2/TNC tumors (Figure S2M), quantification of combined NG2 and CD31 staining signals revealed a 23.7% reduced ratio of NG2 over CD31 in RT2/TNC tumors (Figure 1K), which is indicative of a reduced pericyte coverage of vessels (Song et al., 2005). Finally, we assessed vessel functionality by analyzing fibrinogen (FBG) leakage in tumors upon PBS perfusion of tumor vessels followed by FBG staining (Huijbers et al., 2010) (Figure S2N). Whereas FBG leakage was slightly increased (close to significance, $p = 0.064$) in RT2/TNC over control tumors (Figures 1L and S2O), this analysis revealed a 1.7-fold significantly reduced FBG staining in RT2/TNCKO tumors over RT2 wild-type tumors (Figures 1M and S2P).

Altogether, our results suggest that, whereas TNC promotes the angiogenic switch and increases tumor blood vessel density, it decreases vessel coverage by pericytes and increases leakage, thus perturbing tumor vessel functionality.

Tenascin-C Increases Lung Micrometastasis

In a C57Bl/6 background, RT2 mice do not exhibit macroscopically visible metastasis. To address whether TNC had an effect on micrometastasis formation, we determined expression of insulin (as tumor cell-specific marker) in liver and lung tissue of tumor-bearing mice. Upon tissue staining, we detected cohorts of insulinoma cells within liver and lung tissue confirming their metastatic nature (Figures 2A and S3A). Hematoxylin and eosin (H&E) staining revealed their parenchymal localization. In a subset of mice, we compared quantification of insulin by immunostaining and quantitative RT-PCR (qRT-PCR). This showed a good correlation between both methods and indicates that quantification by qRT-PCR reflects parenchymal localization of micrometastasis rather than circulating tumor cells. We then analyzed a larger sample size of liver and lung tissue by qRT-PCR. Although we did not observe differences in liver tissue between genotypes (Figures S3B and S3C), *insulin* mRNA levels in lungs of RT2/TNC mice were 5.4-fold higher in comparison to lungs of RT2 controls (Figure 2B). Moreover, we observed 28.3-fold lower *insulin* mRNA levels in lungs of mice lacking TNC in comparison to control littermates carrying one TNC allele

Cell PRESS
Open ACCESS

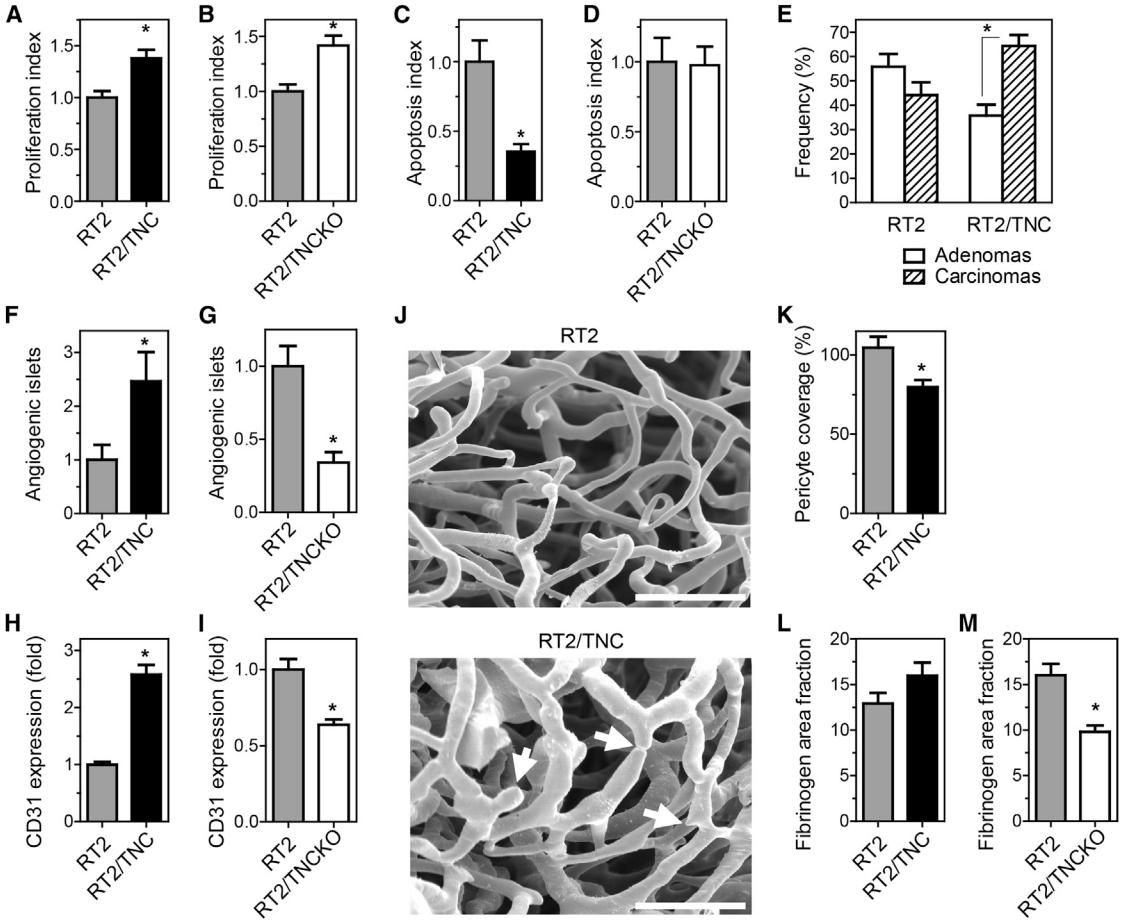

Figure 1. TNC Enhances Proliferation, Survival, and Tumor Progression in RT2 Tumors

(A and B) Quantification of proliferating cells in tumor sections as PH3-positive nuclei in 12-week-old mice. (A) RT2 (n = 9 mice, n = 150 islets), RT2/TNC (n = 8, n = 140). (B) RT2 (n = 6, n = 131) and RT2/TNCKO (n = 6, n = 137).

(C and D) Quantification of apoptotic cells as cleaved caspase-3-positive cells in tumor sections of 12-week-old mice. (C) RT2 (n = 6 mice, n = 84 islets), RT2/TNC (n = 8, n = 123). (D) RT2 (n = 4, n = 95) and RT2/TNCKO (n = 4, n = 83).

(E) Tumor grading into adenoma or invasive carcinoma (H&E-stained tumor sections) of RT2 tumors (n = 26 mice, 78 adenomas, 79 carcinomas) and RT2/TNC (n = 22, 44 adenomas, 76 carcinomas). See Table S1.

(F and G) Number of angiogenic islets per mouse normalized to RT2 controls. See Table S2.

(H and I) Tumor blood vessel quantification upon CD31 staining of tumor sections from 12-week-old mice as CD31-positive area fraction per tumor normalized to RT2 controls. (H) RT2 (n = 6 mice, n = 34 tumors, 203 images) and RT2/TNC (n = 4, n = 17, 106 images). (I) RT2 (n = 3, n = 71) and RT2/TNCKO (n = 3, n = 111).

(J) Morphology of the tumor vasculature in Mercox perfusion casts from 12-week-old RT2 and RT2/TNC mice. Arrows point at break point, branching, and constriction. Scale bars, 50 μm.

(K) Pericyte coverage of tumor blood vessels upon quantification of the ratio of NG2 over CD31 staining signals. RT2 (n = 6 mice, n = 155 tumors) and RT2/TNC (n = 8, n = 204).

(L and M) Quantification of tumor blood vessel leakage upon fibrinogen staining of tumor sections from 12-week-old mice as fibrinogen-positive area fraction per tumor. (L) RT2 (n = 5 mice, n = 62 tumors) and RT2/TNC (n = 3, n = 50). (M) RT2 (n = 4, n = 60) and RT2/TNCKO (n = 5, n = 125). Error bars represent SEM. *$p < 0.05$. See also Figures S1 and S2 and Tables S1 and S2.

(Figure 2C). Our results suggest that in the RT2 model TNC does not affect liver metastasis but increases lung micrometastasis formation.

TNC Expression Correlates with Low Dkk1 Levels and Increases Wnt Target Gene Expression

Because we had noticed downregulation of the Wnt pathway inhibitor DKK1 in T98G glioblastoma cells cultivated on a TNC-containing substratum (Ruiz et al., 2004), we assessed a potential impact of TNC on Dkk1 expression in tumors of the different RT2 genotypes. By qRT-PCR, we noticed that 12 times more RT2/TNC tumors (46.1%) lacked *Dkk1* expression as compared to RT2 controls (3.7%) (Figure 3A). In RT2/TNC tumors with detectable *Dkk1* expression, the levels were 16.1-fold reduced in comparison to RT2 controls (Figure 3B). In contrast, *Dkk1* levels were 2.6-fold higher in tumors lacking TNC as compared to control tumors with one TNC allele (Figure 3C). These observations demonstrate an inverse correlation between TNC and

Cell PRESS
Open ACCESS

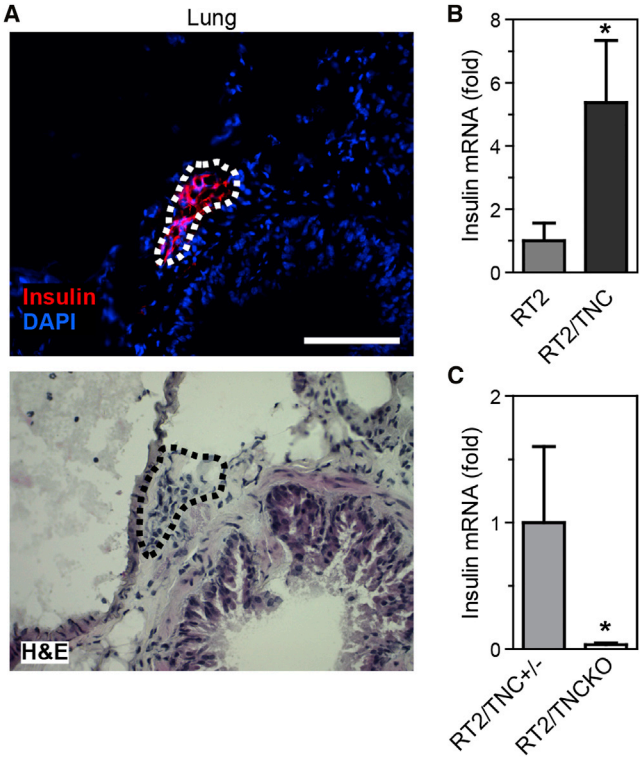

Figure 2. Lung Micrometastasis in RT2 Mice

Insulin expression in a lung RT2 micrometastasis (A) and quantification by qRT-PCR (B and C). (A) Detection of metastasized insulin-positive tumor cells in lung parenchyma (RT2 mouse) by immunostaining (upper panel) and H&E staining (adjacent section, lower panel). Scale bar 50 μm. Detection of insulin expression in RT2 (9/24) and RT2/TNC mice (11/24) (B) and in RT2/TNC$^{+/-}$ (8/13) and RT2/TNCKO littermates (4/13) (C). Error bars represent SEM. *p < 0.05. See also Figure S3.

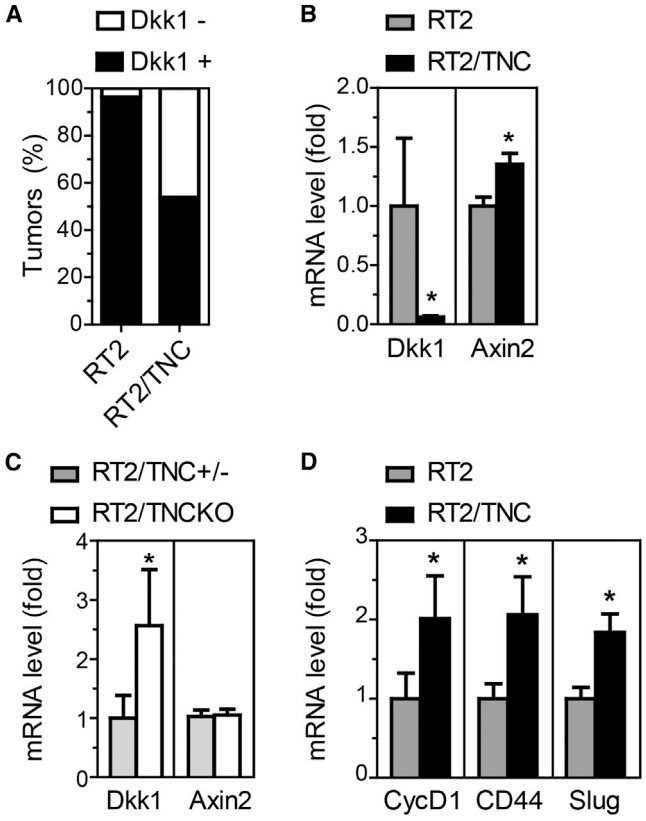

Figure 3. Dkk1 Expression in RT2 Tumors

(A) Tumors were stratified according to *Dkk1* levels, as Dkk1 expressing (Dkk1^{+}) or not expressing (Dkk1^{-}). *Dkk1* was found to be expressed in 26 of 27 RT2 tumors and in 7 of 13 RT2/TNC tumors. Difference between genotypes, $p < 0.05$.

(B) Dkk1 expression was largely reduced in those RT2/TNC tumors with detectable *Dkk1* expression. *Axin2* expression was enhanced in RT2/TNC tumors.

(C) In RT2/TNCKO tumors (15 of 24 tumors were Dkk1 positive) Dkk1 expression was higher compared to RT2/TNC$^{+/-}$ tumors (16 of 23 tumors were Dkk1 positive). Axin2 expression was not changed.

(A–C) *Dkk1* and *Axin2* expression was analyzed by qRT-PCR.

(A–D) Wnt target gene expression in all RT2/TNC and RT2/TNCKO tumors (A–C) or in small differentiated tumors (D), see Table S3. Error bars represent SEM. *p < 0.05.

Dkk1 expression and suggest that TNC may activate Wnt signaling through *Dkk1* repression. To address this possibility, we determined the expression of Wnt target genes by qRT-PCR. We observed an increased expression of the bona fide Wnt signaling target *Axin2* (1.4-fold) in RT2/TNC tumors (Figure 3B), whereas its expression was unchanged in RT2/TNCKO tumors (Figure 3C). This result suggested that ectopic TNC expression induced Wnt signaling, prompting us to analyze expression of other Wnt target genes. Indeed, other Wnt targets such as *Cyclin D1* (2.0-fold), *CD44* (2.0-fold), and *Slug* (1.8-fold) were upregulated in small differentiated tumors of RT2/TNC mice (Figure 3D; Table S3). These results suggest that TNC may contribute to Wnt signaling activation in RT2/TNC tumors through downregulation of the inhibitor Dkk1.

Wnt Activation and DKK1 Inhibition by TNC in Cultured Tumor and Stromal Cells

We then designed in vitro experiments to evaluate a potential Wnt activation by TNC involving DKK1. We used a Wnt reporter (TOPFlash) assay where the expression of the *luciferase* gene is driven by a promoter containing TCF/LEF binding sites. Upon growth of Wnt-3A-stimulated osteosarcoma KRIB cells on a TNC-containing substratum, we observed a 3.5-fold increased Wnt reporter activity (Figure 4A) and a 2.0-fold increased expression of *AXIN2* (Figure 4B), demonstrating that TNC activates the Wnt pathway.

Next, we determined whether TNC affects secretion of soluble factors regulating Wnt signaling in KRIB cells. Therefore, we measured Wnt reporter activity of Wnt-3A-stimulated KRIB cells upon incubation with conditioned medium (CM) from the same cells previously grown on fibronectin (FN) or FN/TNC and observed that, indeed, Wnt activity was higher with CM from cells cultured in the presence of TNC (Figure 4C). These results suggest that TNC activates Wnt signaling through modulating the secretion of activators or inhibitors of the Wnt pathway.

To address whether Wnt inhibitors are regulated by TNC, we investigated their expression by qRT-PCR in cells grown on FN/TNC and FN. Although some inhibitors (*DKK4* and *SFRP2*)

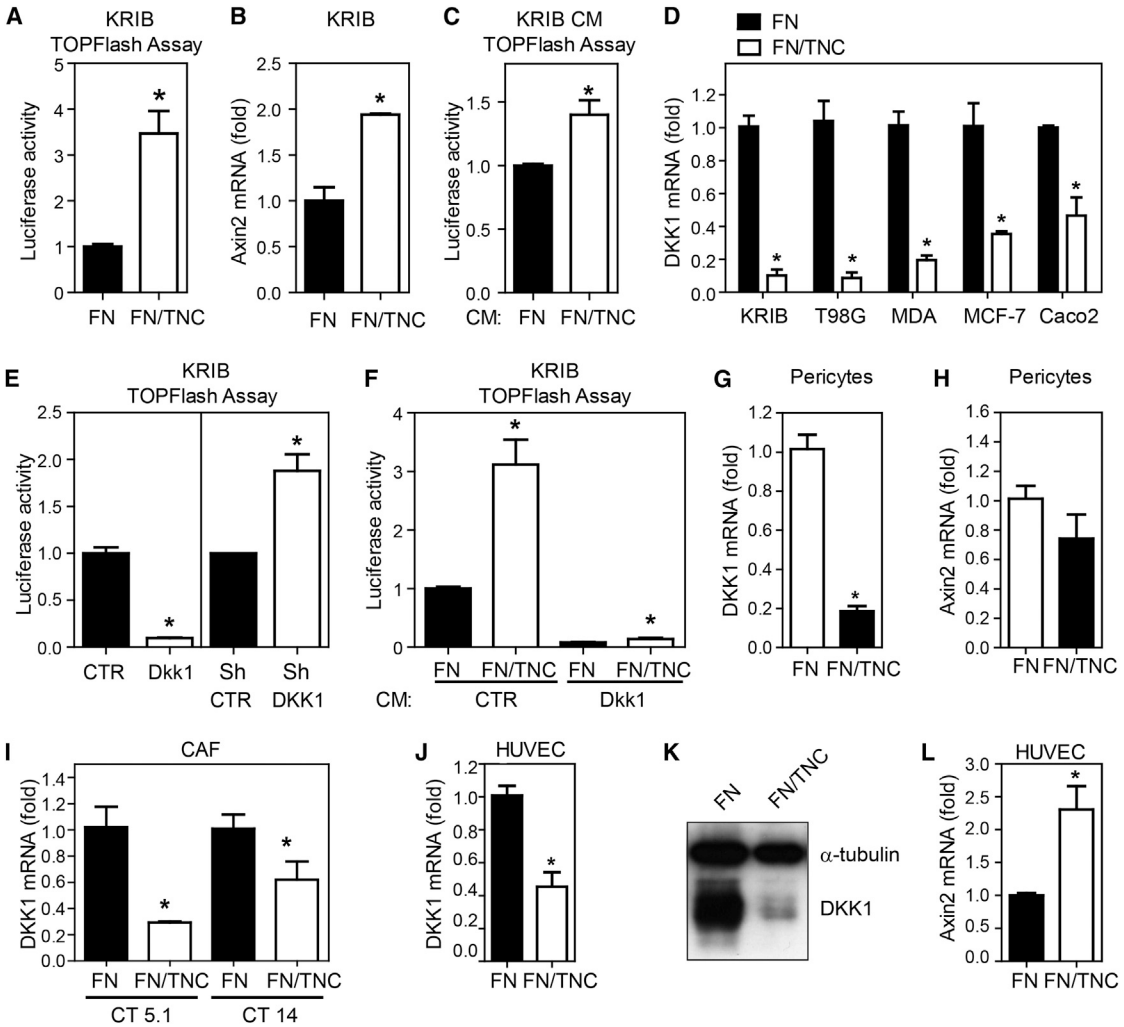

Figure 4. TNC Leads to DKK1 Downregulation and Wnt Signaling Activation in Tumor Cells and Endothelial Cells

(A–C) Enhanced Wnt signaling in Wnt-3A-treated KRIB cells by TNC. TOPFlash activity of cells grown on FN or FN/TNC for 48 hr (A) or treated for 48 hr with Wnt-3A CM and CM of cells grown on FN or FN/TNC (C). (B) *AXIN2* mRNA levels (qRT-PCR, 5 hr).

(D) *DKK1* expression (qRT-PCR, 24 hr) in the indicated tumor cell lines (KRIB, T98G, MDA-MB-435 [MDA], MCF-7, and Caco2) on FN/TNC is represented relative to its expression on FN.

(E) Cell autonomous impact of low (knockdown) and high (overexpression) DKK1 on Wnt signaling as analyzed by TOPFlash activity after 48 hr.

(F) Repression of TNC-mediated Wnt signaling activation by Dkk1. TOPFlash luciferase activity was performed as in (A) except the addition of CM from KRIB control or Dkk1-overexpressing cells after 5 hr of cell seeding on the indicated substrata. Note that the TNC-containing substratum still induced Wnt signaling activity in presence of Dkk1-containing CM, but to a lesser extent (1.8-fold) than in the control conditions (3.1-fold).

(G–I) *DKK1* and *Axin2* mRNA levels in pericytes (G and H) and two human colorectal-cancer-derived CAF primary lines (I) seeded on FN or FN/TNC (5 hr). TNC leads to downregulation of *DKK1* in pericytes and CAFs (G and I), but *AXIN2* expression remains unchanged in pericytes (H).

(J–L) Enhanced Wnt signaling by TNC in HUVECs. qRT-PCR for DKK1 and AXIN2 (5 hr) (J and L) and DKK1 immunoblotting (24 hr) (K). Data from three independent experiments (except D: MCF-7 and Caco2 cell lines, one and two experiments, respectively; and I: two experiments) are shown as mean ± SEM. *$p < 0.05$. See also Figure S4.

were not expressed, no consistent effect of TNC was observed on the expression of other analyzed Wnt inhibitors (*DKK2*, *DKK3*, *SFRP1*, *SFRP3*, *SFRP4*) in KRIB, T98G, and MDA-MB435 cells (Figure S4A). In contrast, we observed a robust downregulation of *DKK1* in all five analyzed tumor cell lines of different origin after 24 hr on the TNC-containing substratum (Figures 4D and S4A). DKK1 downregulation was observed at both RNA and protein levels, with a fast (5 hr) and long-lasting (up to 12 days) effect in T98G cells (Figures S4B and S4C).

To determine whether modulation of DKK1 expression contributes to TNC-dependent Wnt signaling in KRIB cells, TOPFlash activity was measured upon overexpression and knockdown of DKK1, respectively (Figures S4D–S4G). Indeed, activity of the Wnt signaling reporter was DKK1 dependent because it was increased upon DKK1 knockdown and decreased upon Dkk1 overexpression (Figure 4E) and was repressed by Dkk1-containing CM in a dose-dependent manner (Figure S4H). When KRIB cells were incubated with Dkk1 CM on

Please cite this article in press as: Saupe et al., Tenascin-C Downregulates Wnt Inhibitor Dickkopf-1, Promoting Tumorigenesis in a Neuroendocrine Tumor Model, Cell Reports (2013), http://dx.doi.org/10.1016/j.celrep.2013.09.014

Cell PRESS
Open ACCESS

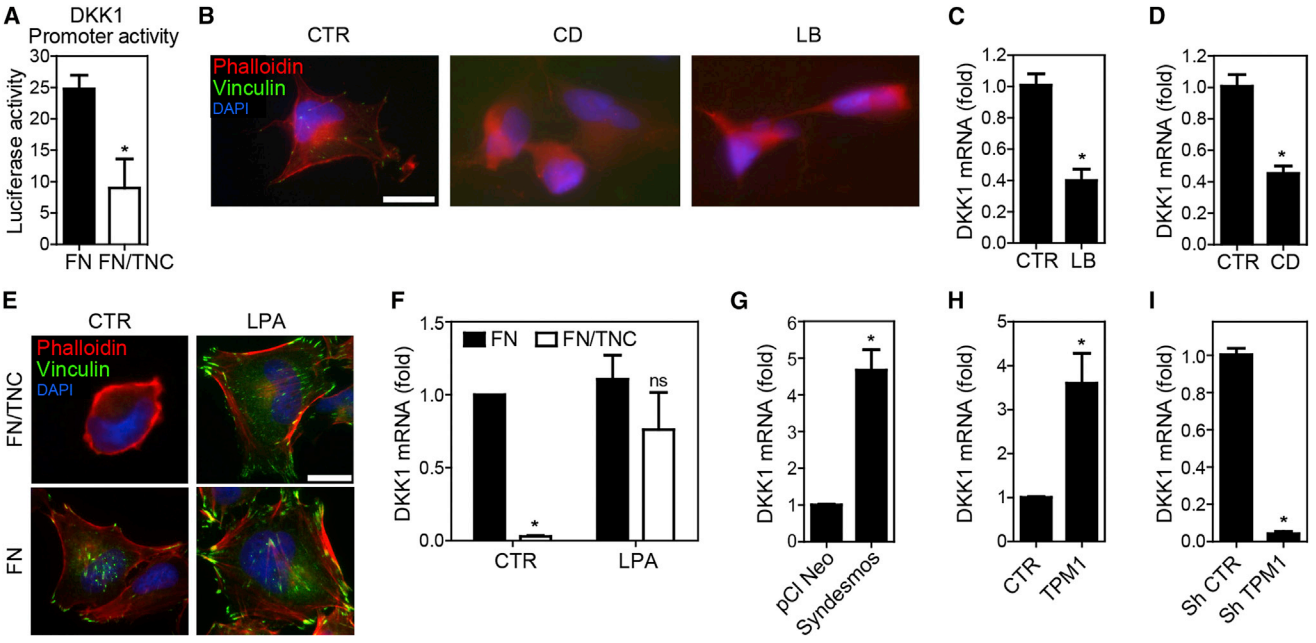

Figure 5. Mechanism of DKK1 Downregulation

(A) Reduced *DKK1* promoter activity by TNC. *DKK1* promoter driven luciferase activity in T98G cells is shown upon growth for 48 hr on the indicated substrata.

(B and E) Phalloidin (red) and vinculin (green) stainings of serum-starved T98G cells upon CTR, CD (2 μM), or LB (5 μM) treatment for 3 hr (B). Nuclei are stained in blue (DAPI). Scale bar 20 μm.

(C and D) *DKK1* mRNA levels in serum-starved T98G upon LB (5 μM, 3 hr) (C) or CD (2 μM, 3 hr) (D) treatment.

(E) IF staining of T98G cells upon control or LPA (30 μM) treatment. Serum-starved T98G were plated on fibronectin (FN) or fibronectin/tenascin-C (FN/TNC), and after 1 hr LPA was added for 4 hr. Although cells are poorly spread under control conditions on FN/TNC (no actin stress fibers, few focal adhesions), LPA treatment restored cell spreading associated with the formation of focal adhesions and actin stress fibers. Scale bar, 20 μm.

(F) *DKK1* mRNA expression determined by qRT-PCR upon treatment with 30 μM LPA. LPA restores *DKK1* expression on FN/TNC.

(G–I) *DKK1* mRNA expression determined by qRT-PCR upon ectopic expression of chicken syndesmos (G) and mouse TPM1 (H) or upon knockdown of TPM1 (I). Syndesmos or TPM1 overexpression induces *DKK1* mRNA expression, whereas TPM1 knockdown leads to *DKK1* downregulation.

Data are shown as mean ± SEM. *$p < 0.05$. See also Figure S5.

FN/TNC and FN, Wnt reporter activity was largely reduced (Figure 4F), suggesting that TNC-induced repression of DKK1 facilitates Wnt pathway activation.

Next, we determined whether stromal cells also downregulated DKK1 on a TNC substratum. Therefore, *DKK1* expression was determined in two monocytic/macrophage cell lines, primary human brain pericytes, two colorectal cancer derived carcinoma associated fibroblasts (CT5.1, CT14), and human umbilical vein endothelial cells (HUVECs) upon growth on FN/TNC and FN. We noticed that in contrast to the two macrophage lines that did not at all express *DKK1*, pericytes (5-fold), CAFs (3.0- and 1.6-fold), and HUVECs (2.2-fold) significantly downregulated DKK1 mRNA (Figures 4G, 4I, and 4J) and protein (Figure 4K) on a TNC substratum. Whereas *Axin2* expression was not affected in pericytes (Figure 4H), *Axin2* mRNA was 2.3-fold increased in HUVECs on FN/TNC in comparison to FN (Figure 4L). Altogether, our results show that TNC induces downregulation of DKK1 in tumor and stromal cells and activates Wnt signaling in tumor and endothelial cells.

Mechanism of DKK1 Downregulation by TNC

First, we determined whether *DKK1* mRNA stability is substratum dependent. Therefore, T98G cells were treated with the RNA polymerase II inhibitor Actinomycin D, but DKK1 mRNA levels were equally low in cells on FN and FN/TNC, suggesting that *DKK1* is not regulated by mRNA stabilization (Figure S5A). Next, we addressed whether TNC downregulates DKK1 at transcriptional level. Therefore, we performed reporter assays by measuring luciferase activity under control of a 3.2 kb *DKK1* promoter sequence. Indeed, we observed a 2.5-fold reduced *DKK1* promoter activity in cells grown for 48 hr on a TNC-containing substratum (Figure 5A).

Because TNC blocks actin stress fiber formation (Huang et al., 2001; Midwood et al., 2004; Murphy-Ullrich et al., 1991; Orend et al., 2003), we investigated whether disruption of the actin cytoskeleton has an impact on *DKK1* mRNA levels. Treatment with Latrunculin B (LB) and Cytochalasin D (CD) disrupted actin stress fibers and focal adhesions and, importantly, reduced *DKK1* expression (Figures 5B–5D). To address the converse whether more actin stress fibers stimulate *DKK1* expression, we treated KRIB and T98G cells with lysophosphatidic acid (LPA) and observed an increased and dose-dependent *DKK1* mRNA expression similar to serum response factor (SRF), a known actin stress fiber-regulated gene (Gineitis and Treisman, 2001; Spencer and Misra, 1999) (Figures S5B–S5F). Moreover, LPA (30 μM) restored cell spreading, actin stress fibers, and focal

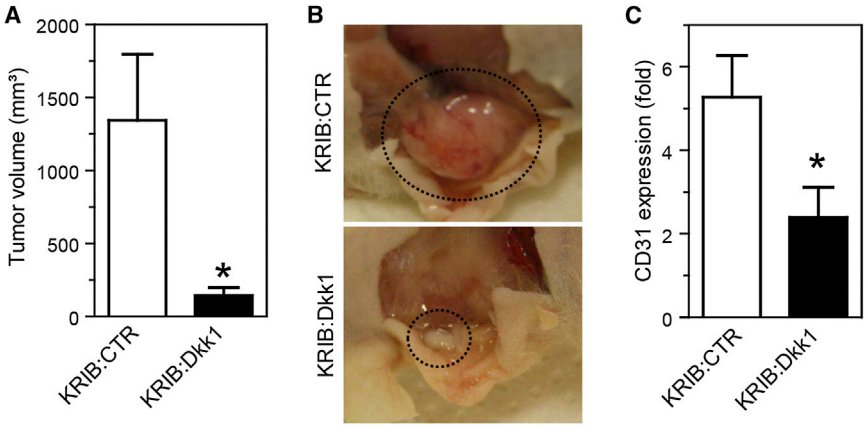

Figure 6. Dkk1 Overexpression Inhibits Osteosarcoma Growth and Angiogenesis

(A) Mean tumor volume of control (CTR, n = 10) and Dkk1-overexpressing (n = 9) KRIB tumors upon subcutaneous injection of the corresponding cells into nude mice.

(B) Representative tumor images.

(C) Tumor microvessel density, as determined by CD31 staining and quantification, was 2.2-fold reduced in KRIB:Dkk1 tumors (n = 8) as compared to control KRIB tumors (n = 10).

Error bars represent SEM. *p < 0.05. See also Figure S6.

adhesions in T98G cells on a FN/TNC substratum and most importantly largely restored *DKK1* levels on this substratum to that on FN (Figures 5E and 5F). Because LPA can trigger RhoA signaling (Mills and Moolenaar, 2003), and RhoA expression (Lange et al., 2007) and function (Wenk et al., 2000) are impaired by TNC, we determined whether overexpression of a constitutively active (CA) RhoA molecule impacts on *DKK1* expression. Whereas, CA-RhoA increased SRF target gene expression (Figures S5G–S5J), it did not alter *DKK1* expression (Figures S5K and S5L), suggesting that LPA triggers *DKK1* expression by a RhoA-independent pathway.

Because tropomyosin-1 (TPM1) and syndesmos overexpression bypass the cell adhesion blocking and actin stress-fiber-disrupting effect of TNC on a FN/TNC substratum (Lange et al., 2008), we determined whether ectopic expression of syndesmos and TPM1 have an impact on *DKK1* expression. Whereas shTPM1 blocked *DKK1* expression, overexpression of syndesmos and TPM1 increased *DKK1* mRNA levels to 4.7- and 3.6-fold, respectively (Figures 5G–5I and S5M–S5P).

Altogether, these results demonstrated that *DKK1* expression is regulated at the promoter level and that actin stress fibers and focal adhesion signaling drive *DKK1* transcription independently of RhoA. We conclude that TNC downregulates *DKK1* transcription by blocking focal adhesion and actin stress fiber formation.

Repression of Tumor Angiogenesis by DKK1

As we observed that TNC promotes tumor angiogenesis and downregulates *DKK1* expression, we addressed whether DKK1 impacts on tumor angiogenesis in xenografted tumors of KRIB cells with different DKK1 levels. We found that upon Dkk1 overexpression (Figure S6A) tumors were significantly smaller (Figure 6A) and pale (Figure 6B). Quantification of microvessel density upon CD31 staining revealed that Dkk1-overexpressing tumors were less vascularized (Figure 6C), suggesting that Dkk1 overexpression impaired tumor angiogenesis. In addition, conditioned medium from KRIB cells overexpressing Dkk1 inhibited HUVEC tubulogenesis on Matrigel in vitro (Figure S6D). We addressed whether Dkk1 potentially had an impact on tumor growth through inhibiting tumor cell proliferation and found no statistically significant difference in proliferation in cultured cells or in the tumors with elevated Dkk1 levels (Figures S6B and S6C).

Because Dkk1 influenced proliferation of tumor cells neither in vitro nor in vivo, our data suggest that Dkk1 overexpression impairs angiogenesis and thereby inhibits KRIB tumor growth. Because DKK1 blocks angiogenesis in a VEGFA context (Min et al., 2011), we investigated whether full-length TNC binds VEGFA. Indeed, by surface plasmon resonance we observed a dose-dependent binding of VEGFA to TNC (Figure S7), extending data on binding of VEGFA to the fifth FNIII domain in TNC (De Laporte et al., 2013) by providing a K_d of 2.7×10^{-7} M, which is in the range of a VEGFA/glycosaminoglycan interaction (2.4×10^{-8} M) (Wu et al., 2009).

TNC Expression in Human Insulinomas

As we demonstrated a tumor-promoting effect of TNC in the murine RT2 insulinoma model, we assessed a potential clinical relevance by determining TNC expression in human insulinomas using qRT-PCR and immunohistochemical staining of patient tumor tissue. Of note, insulinomas are rare and most are benign, yet a few (10%–15%) metastasize to lymph nodes and liver (Metz and Jensen, 2008). At RNA level, we found that *TNC* expression was detectable in all analyzed human insulinomas (Figure 7A). Most importantly, we observed the highest *TNC* expression levels (3/14) in tumors from patients with metastasis to liver or lymph nodes (Figures 7A and 7B), suggesting that a high TNC expression correlates with metastasis formation in human insulinomas.

DISCUSSION

We have used the RT2 model of multistage pancreatic β-cell tumorigenesis with abundant and no TNC expression to obtain a better understanding of TNC contribution to tumor progression and we have observed multiple effects. Enhanced TNC levels in TNC transgenic RT2 mice correlate with an increase in tumor cell proliferation and survival, carcinoma formation, angiogenesis, and lung micrometastasis. On the contrary, the absence of TNC results in reduced angiogenesis and lung micrometastasis. These results confirm a crucial role of TNC in tumor progression as has been suspected in human cancer.

There is much evidence for an important role of TNC in promoting tumor angiogenesis (Midwood et al., 2011). However, despite the fact that TNC has been extensively investigated for almost three decades (Chiquet-Ehrismann et al., 1986), it is not

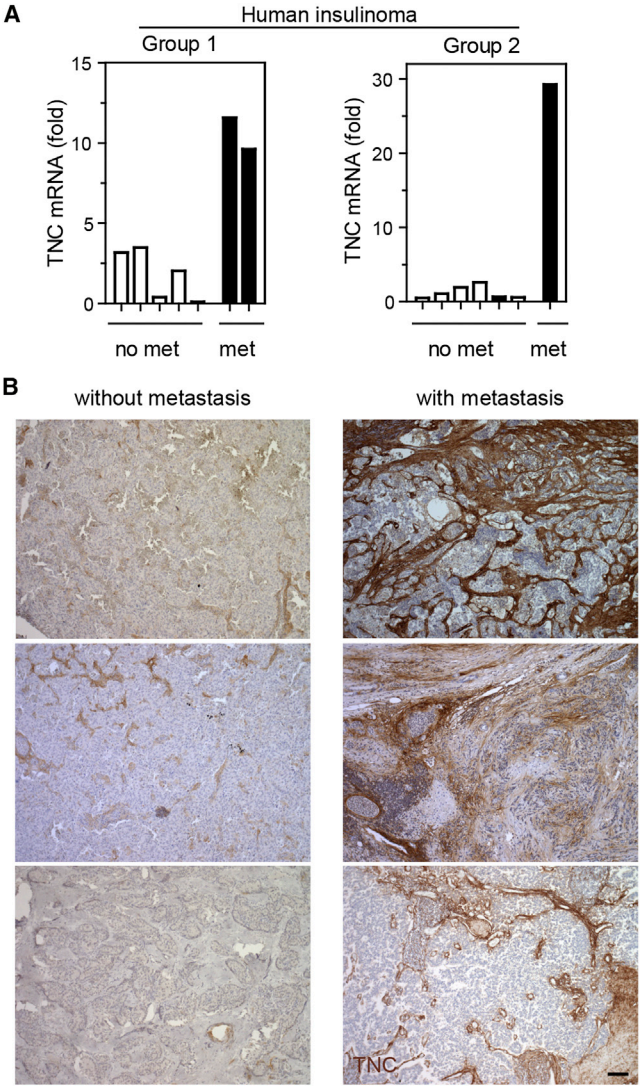

Figure 7. TNC Expression Correlates with Metastasis Formation in Human Insulinomas

(A) *TNC* mRNA expression was determined by qRT-PCR in two patient groups (group 1, Munich cohort; group 2, Strasbourg cohort) and is displayed as relative expression upon normalization to *GAPDH*. Upon combining data of the two groups, *TNC* expression in patients with metastasis is increased over that in patients without metastasis ($p < 0.05$).

(B) TNC expression was determined by IHC in all tumors of the two groups of insulinomas. Representative pictures of the three metastatic and three non-metastatic insulinomas are shown. Scale bar, 100 μm.

resolved how TNC impacts tumor angiogenesis at the molecular level. Whereas TNC can have stimulatory effects on endothelial cell migration, conflicting reports exist concerning its impact on tubulogenesis. A proangiogenic effect of TNC linked to VEGFA expression was seen in human melanoma xenografts implanted into immune-compromised mice lacking TNC (Tanaka et al., 2004). Of note, in the RT2/TNC tumors we did not observe an increased *VEGFA* expression (M.K., F.S., G.O., unpublished data). Our study addresses the role of TNC on tumor angiogenesis systematically by using a stochastic genetic tumor model with an intact immune system. Here, we investigated the angiogenic switch, tumor blood vessels, and their functionality. Most importantly, our study shows that TNC promotes the angiogenic switch, a rate-limiting step along tumor progression (Hanahan and Folkman, 1996), and the abundance of endothelial cells. However, TNC seems to impair vessel functionality because tumor vessels of RT2/TNC mice are morphologically aberrant and less covered by pericytes. Moreover, vessels in RT2 tumors lacking TNC are less leaky than those with TNC, suggesting a role of TNC in the formation of more but less functional tumor vessels.

We have identified DKK1 as an important TNC target in RT2 tumors. Our in vivo and in vitro results suggest that TNC promotes tumor progression involving DKK1 downregulation and activation of Wnt signaling. First, the *TNC* copy number inversely correlates with *DKK1* expression in RT2 tumors, and a TNC substratum downregulates *DKK1* expression in tumor and several stromal cell types (CAFs, pericytes, and endothelial cells). Second, Wnt signaling is increased by TNC in the RT2 model and in cultured endothelial and tumor cells. Third, TNC-induced Wnt activation is reduced in tumor cells by DKK1. Finally, downregulation of *DKK1* by TNC may be a key event because no other major Wnt inhibitor is consistently regulated by a TNC-containing substratum (our data; Ruiz et al., 2004).

Several transcriptional regulators, epigenetic silencing, and tissue tension were shown to regulate DKK1 expression (Aguilera et al., 2006; Barbolina et al., 2013; Liao et al., 2008; Menezes et al., 2012; Pendás-Franco et al., 2008; Zhou et al., 2012). Here, we demonstrate that TNC downregulates *DKK1* expression by promoter inhibition. Because TNC blocks actin stress fiber formation (Huang et al., 2001; Midwood et al., 2004; Murphy-Ullrich et al., 1991; van Obberghen-Schilling et al., 2011), we investigated whether *DKK1* expression is regulated by the actin polymerization state and demonstrated that TPM1 antisense and drug-induced disruption of the actin cytoskeleton reduced *DKK1* mRNA levels. On the contrary, enforcing actin polymerization and stress fiber formation by overexpression of syndesmos, bridging integrin $\alpha5\beta1$ and syndecan-4 in focal adhesions (Bass and Humphries, 2002), largely increased *DKK1* expression. We further showed that LPA rescued focal adhesion and actin stress fiber formation and cell spreading on FN/TNC, which we linked to restored *DKK1* expression in a RhoA-independent manner. How TNC downregulates *DKK1* expression at promoter level is currently unknown and requires further investigation, but it does not appear to be exclusively dependent on the SRF cotranscription factor MKL1 that is regulated by actin polymerization (Miralles et al., 2003) (A.S. and G.O., unpublished data). Previously, it was shown that a stiffened collagen substratum, implicating integrin adhesion signaling (Levental et al., 2009), induces *DKK1* downregulation in several cell types including endothelial cells (Barbolina et al., 2013). Here, we report a mechanism whereby TNC blocks *DKK1* transcription through disruption of actin stress fibers.

The role of DKK1 in developmental and tumor angiogenesis appears to be context dependent, because DKK1 can produce pro- and antiangiogenic effects (Aicher et al., 2008; De Langhe et al., 2005; Min et al., 2011; Oh et al., 2012; Reis

et al., 2012; Smadja et al., 2010). Interestingly, the growth factor context seems to be particularly critical for the outcome, because, for example, DKK1 promotes basic fibroblast-growth-factor-induced angiogenesis (Aicher et al., 2008; Reis et al., 2012; Smadja et al., 2010) but blocks VEGFA-induced (Min et al., 2011) angiogenesis in Matrigel plug assays in vivo. We here confirm that DKK1 inhibits HUVEC tubulogenesis in vitro (Min et al., 2011) and tumor angiogenesis in an osteosarcoma xenograft model in vivo.

Employing the RT2 model, we show that TNC promotes metastasis formation to the lung but not to the liver. This is reminiscent of breast cancer where TNC is part of a gene expression signature specifically associated with lung but not bone metastasis (Minn et al., 2005), an initial observation that has been subsequently confirmed and functionally validated using xenograft models (Oskarsson et al., 2011; Tavazoie et al., 2008). Mechanistically, TNC expression was linked to an increased tumor cell survival and activation of Wnt and Notch signaling, as revealed by increased expression of Lgr5 and Msi1, respectively (Oskarsson et al., 2011). Although we have shown that Wnt signaling is activated in TNC-overexpressing RT2 tumors and in cellular models comprising tumor and endothelial cells in vitro, the expression of Lgr5 and of several Notch pathway members are unaffected in the in vivo and in vitro models we used (Table S3; F.S. and G.O., unpublished data). Multiple explanations for these differences may exist, such as difference in model systems and in organ and tissue context. We have shown that the ectopic expression of TNC leads to *DKK1* downregulation and Wnt signaling activation in RT2/TNC tumors as revealed by the upregulation of other Wnt target genes, including the prototypical Wnt target *Axin2*. Conversely, in RT2/TNCKO tumors DKK1 levels were increased, but *Axin2* expression was unchanged. This result is in line with a previous report showing that the Wnt pathway has minimal basal activity in pancreatic beta tumor cells and is dispensable for RT2 tumor progression (Herzig et al., 2007). In addition to canonical Wnt signaling, the DKK1 receptor LRP6 was shown to promote PDGF-BB, TGF-β and CTGF signaling in pericytes and fibroblasts. Importantly, these signaling activities were blocked by DKK1 through binding to LRP6 (Ren et al., 2013). We suggest that a TNC-rich matrix induces a microenvironment with low DKK1 levels that is susceptible to angiogenic signaling from Wnt and other pathways regulated by DKK1. This possibility is supported by our results that have shown an inverse correlation of TNC and DKK1 expression, promotion of the angiogenic switch by TNC, and a strong downregulation of DKK1 by TNC in tumor and several stromal cell types.

In the TNC transgenic RT2 model, we observed that TNC promotes multiple early events such as proliferation and survival in hyperplastic islets, Wnt target upregulation in small, differentiated tumors, and the angiogenic switch. A major role of TNC early in tumorigenesis combined with a less functional vasculature may explain why macroscopically visible RT2 tumors of the different genotypes did not differ in size. A potential early role of TNC in tumorigenesis has not received much attention because cancer patient data with a correlation of high TNC expression and malignancy (Midwood and Orend, 2009; Oskarsson et al., 2011) rather suggested a major role of TNC in late events. In human cancer tissue, early events cannot be easily addressed, which might explain why we did not see a correlation of *TNC* and *DKK1* mRNA expression levels in human cancer tissues. TNC promotes metastasis (Minn et al., 2005; Oskarsson et al., 2011; Tavazoie et al., 2008), which has also been recapitulated here in the RT2 model and in human insulinomas where the highest TNC expression levels were observed in the few available metastatic insulinomas.

In summary, we have shown that DKK1 expression is dependent on actin stress fibers that are disrupted by TNC. We have established a transgenic immune-competent tumor mouse model that mimics the high expression of TNC observed in human cancer. Our results prove that TNC plays crucial roles along tumor progression by promoting early and late events. We demonstrate that TNC levels determine the extent of tumor cell survival, invasion, tumor angiogenesis, and metastasis. These phenotypes appear to be linked to DKK1 downregulation creating a proangiogenic tumor microenvironment. Finally, our human TNC-expressing transgenic tumor mice offer a model for human insulinoma progression and for the preclinical evaluation of drugs that target human TNC.

EXPERIMENTAL PROCEDURES

Mice

Generation of transgenic RipTNC mice, breeding, genotyping, xenograft experiments, and analysis of tumor material are specified in the Supplemental Information. RT2 mice developing pancreatic neuroendocrine tumors (Hanahan, 1985) were crossed with RipTNC (this study) or TNCKO (Forsberg et al., 1996) mice to generate double-transgenic mice with forced expression of TNC (RT2/TNC) or lacking TNC expression (RT2/TNCKO). Experiments comprising animals were performed according to the guidelines of INSERM and the Swiss Federal Veterinary Office.

Histopathological Analysis of Mouse and Human Tissue

Tumor incidence per mouse was determined as the number of all visible tumors with a minimal diameter of 1 mm. Tumor volume was calculated assuming a spherical shape with formula $V = 1/6 \times \pi \times d^3$ (d = tumor diameter). Pancreata, liver, and lung tissue were isolated, fixed in 4% paraformaldehyde (PFA) overnight followed by embedding in paraffin, fixed for 2 hr in 4% PFA, immersed in 20% sucrose overnight, and embedded in Tissue-Tek O.C.T. (Sakura Finetek) or freshly embedded in O.C.T. and frozen on dry ice.

Histological analysis was performed on 5 μm (paraffin embedded) and 7 μm (cryopreserved) tissue sections by staining with H&E or immunostaining. Primary antibodies were incubated overnight at 4°C. Immunohistochemical (IHC) detection was performed on paraffin-embedded tissue using Vectastain developing system (Vector Laboratories), followed by staining with hematoxilin. Detection by IF was performed on fixed or fresh-frozen tissue using fluorescein-isothiocyanate- or Cy3-coupled secondary antibodies (Jackson ImmunoResearch Laboratories); cell nuclei were stained with DAPI. Primary antibodies detecting the following molecules were used: phosphohistone H3 (PH3, 1:200, Upstate 06-570), cleaved caspase-3 (1:50, Cell Signaling Technology 9661), CD31 (1:50, BD Pharmingen 550274, Acris BM4086), NG2 (1:200, Millipore AB5320), insulin (1:200, Dako Cytomation A0564), glucagon (1:1000, Sigma G2654), KI67 (1:200, clone SP6, Thermo Scientific, RM-9106-S1), human TNC (BC-24, 1:3000, Sigma T2551), and fibrinogen (1:500, Dako A0080). Anti-mouse TNC MTn12 (Aufderheide and Ekblom, 1988) and anti-human TNC B28.13 antibodies (Schenk et al., 1995) were purified from hybridoma culture supernatants.

Quantification of IF microscopic pictures was done using ImageJ (National Institutes of Health) software. Staining protocols (fixation, blocking, antibody dilution) and image acquisition setting (microscope, magnification, light intensity, exposure time) were kept constant per experiment. Data were quantified

as counted events over analyzed tumor area (PH3), as area fraction over analyzed DAPI-positive cell area (cleaved caspase-3, PH3, and KI67) or as area fraction over analyzed tumor area (CD31, NG2, and fibrinogen).

Cell-Culture Experiments

Coating of cell-culture dishes with FN and TNC was performed as described earlier (Huang et al., 2001; Lange et al., 2007). Cells were seeded on the coated surfaces and analyzed using standard protocols as described. mRNA was extracted from paraffin-embedded tissue and analyzed by qRT-PCR.

Human Insulinomas

Tumor material was obtained from the Klinikum rechts der Isar (Munich, Germany) or the Hôpital de Hautepierre (Strasbourg, France). Analysis of the human insulinomas had been approved by the respective ethics committees. All samples were obtained after prior patient informed written consent. Tumor tissue was obtained from 14 patients (group 1, Munich, and group 2, Strasbourg) with endocrine pancreatic cancer and was histopathologically confirmed as insulinoma by an experienced pathologist. Presence of metastasis was diagnosed in three patients (liver or lymph node n = 2, group 1; liver and lymph node n = 1, group 2).

SUPPLEMENTAL INFORMATION

Supplemental Information includes Supplemental Experimental Procedures, seven figures, and three tables and can be found with this article online at http://dx.doi.org/10.1016/j.celrep.2013.09.014.

ACKNOWLEDGMENTS

We thank W. Huang, A.-C. Feutz, K. Strittmatter, H. Antoniadis, P. Lorentz, M.-F. Hamou, B. Scolari, R. Buergy, E. Domany, J. Huelsken, R. Fässler, M. Kedinger, I. Gross, G. Posern, R. Moon, and R. Chiquet-Ehrismann for technical assistance, reagents, mice, discussion, and help with the generation of the transgenic mice. Support was generously provided by the University Strasbourg and the Association pour la Recherche sur le cancer (to A.S.); the Fondation des Treilles (to F.S.); INSERM/Region Alsace (to I.G.); the Ligue contre le Cancer (to O.L., P.S.-A., and G.O.); and INSERM, University Strasbourg, Agence National de la Recherche, Krebsliga Beider Basel, the Association for International Cancer Research, the Swiss National Science Foundation, Oncosuisse, the Novartis Foundation for Biological and Medical Sciences, the Hôpital de Hautepierre, the Association pour la Recherche contre le Cancer, and the Institut National du Cancer (to G.O.).

Received: March 20, 2013
Revised: August 7, 2013
Accepted: September 10, 2013
Published: October 17, 2013

REFERENCES

Aguilera, O., Fraga, M.F., Ballestar, E., Paz, M.F., Herranz, M., Espada, J., García, J.M., Muñoz, A., Esteller, M., and González-Sancho, J.M. (2006). Epigenetic inactivation of the Wnt antagonist DICKKOPF-1 (DKK-1) gene in human colorectal cancer. Oncogene *25*, 4116–4121.

Aguirre-Ghiso, J.A. (2007). Models, mechanisms and clinical evidence for cancer dormancy. Nat. Rev. *7*, 834–846.

Aicher, A., Kollet, O., Heeschen, C., Liebner, S., Urbich, C., Ihling, C., Orlandi, A., Lapidot, T., Zeiher, A.M., and Dimmeler, S. (2008). The Wnt antagonist Dickkopf-1 mobilizes vasculogenic progenitor cells via activation of the bone marrow endosteal stem cell niche. Circ. Res. *103*, 796–803.

Almog, N. (2010). Molecular mechanisms underlying tumor dormancy. Cancer Lett. *294*, 139–146.

Aufderheide, E., and Ekblom, P. (1988). Tenascin during gut development: appearance in the mesenchyme, shift in molecular forms, and dependence on epithelial-mesenchymal interactions. J. Cell Biol. *107*, 2341–2349.

Barbolina, M.V., Liu, Y., Gurler, H., Kim, M., Kajdacsy-Balla, A.A., Rooper, L., Shepard, J., Weiss, M., Shea, L.D., Penzes, P., et al. (2013). Matrix rigidity activates Wnt signaling through down-regulation of Dickkopf-1 protein. J. Biol. Chem. *288*, 141–151.

Bass, M.D., and Humphries, M.J. (2002). Cytoplasmic interactions of syndecan-4 orchestrate adhesion receptor and growth factor receptor signalling. Biochem. J. *368*, 1–15.

Bissell, M.J., and Labarge, M.A. (2005). Context, tissue plasticity, and cancer: are tumor stem cells also regulated by the microenvironment? Cancer Cell *7*, 17–23.

Chiquet-Ehrismann, R., Mackie, E.J., Pearson, C.A., and Sakakura, T. (1986). Tenascin: an extracellular matrix protein involved in tissue interactions during fetal development and oncogenesis. Cell *47*, 131–139.

De Langhe, S.P., Sala, F.G., Del Moral, P.M., Fairbanks, T.J., Yamada, K.M., Warburton, D., Burns, R.C., and Bellusci, S. (2005). Dickkopf-1 (DKK1) reveals that fibronectin is a major target of Wnt signaling in branching morphogenesis of the mouse embryonic lung. Dev. Biol. *277*, 316–331.

De Laporte, L., Rice, J.J., Tortelli, F., and Hubbell, J.A. (2013). Tenascin C promiscuously binds growth factors via its fifth fibronectin type III-like domain. PLoS ONE *8*, e62076.

Forsberg, E., Hirsch, E., Fröhlich, L., Meyer, M., Ekblom, P., Aszodi, A., Werner, S., and Fässler, R. (1996). Skin wounds and severed nerves heal normally in mice lacking tenascin-C. Proc. Natl. Acad. Sci. USA *93*, 6594–6599.

Gineitis, D., and Treisman, R. (2001). Differential usage of signal transduction pathways defines two types of serum response factor target gene. J. Biol. Chem. *276*, 24531–24539.

Glinka, A., Wu, W., Delius, H., Monaghan, A.P., Blumenstock, C., and Niehrs, C. (1998). Dickkopf-1 is a member of a new family of secreted proteins and functions in head induction. Nature *391*, 357–362.

Hanahan, D. (1985). Heritable formation of pancreatic beta-cell tumours in transgenic mice expressing recombinant insulin/simian virus 40 oncogenes. Nature *315*, 115–122.

Hanahan, D., and Folkman, J. (1996). Patterns and emerging mechanisms of the angiogenic switch during tumorigenesis. Cell *86*, 353–364.

Hanahan, D., Christofori, G., Naik, P., and Arbeit, J. (1996). Transgenic mouse models of tumour angiogenesis: the angiogenic switch, its molecular controls, and prospects for preclinical therapeutic models. Eur. J. Cancer *32A*, 2386–2393.

Herzig, M., Savarese, F., Novatchkova, M., Semb, H., and Christofori, G. (2007). Tumor progression induced by the loss of E-cadherin independent of beta-catenin/Tcf-mediated Wnt signaling. Oncogene *26*, 2290–2298.

Huang, W., Chiquet-Ehrismann, R., Moyano, J.V., Garcia-Pardo, A., and Orend, G. (2001). Interference of tenascin-C with syndecan-4 binding to fibronectin blocks cell adhesion and stimulates tumor cell proliferation. Cancer Res. *61*, 8586–8594.

Huijbers, E.J., Ringvall, M., Femel, J., Kalamajski, S., Lukinius, A., Abrink, M., Hellman, L., and Olsson, A.K. (2010). Vaccination against the extra domain-B of fibronectin as a novel tumor therapy. FASEB J. *24*, 4535–4544.

Kerbel, R.S. (2008). Tumor angiogenesis. N. Engl. J. Med. *358*, 2039–2049.

Lange, K., Kammerer, M., Hegi, M.E., Grotegut, S., Dittmann, A., Huang, W., Fluri, E., Yip, G.W., Götte, M., Ruiz, C., and Orend, G. (2007). Endothelin receptor type B counteracts tenascin-C-induced endothelin receptor type A-dependent focal adhesion and actin stress fiber disorganization. Cancer Res. *67*, 6163–6173.

Lange, K., Kammerer, M., Saupe, F., Hegi, M.E., Grotegut, S., Fluri, E., and Orend, G. (2008). Combined lysophosphatidic acid/platelet-derived growth factor signaling triggers glioma cell migration in a tenascin-C microenvironment. Cancer Res. *68*, 6942–6952.

Levental, K.R., Yu, H., Kass, L., Lakins, J.N., Egeblad, M., Erler, J.T., Fong, S.F., Csiszar, K., Giaccia, A., Weninger, W., et al. (2009). Matrix crosslinking forces tumor progression by enhancing integrin signaling. Cell *139*, 891–906.

Liao, Y.L., Sun, Y.M., Chau, G.Y., Chau, Y.P., Lai, T.C., Wang, J.L., Horng, J.T., Hsiao, M., and Tsou, A.P. (2008). Identification of SOX4 target genes using phylogenetic footprinting-based prediction from expression microarrays suggests that overexpression of SOX4 potentiates metastasis in hepatocellular carcinoma. Oncogene *27*, 5578–5589.

Lu, P., Weaver, V.M., and Werb, Z. (2012). The extracellular matrix: a dynamic niche in cancer progression. J. Cell Biol. *196*, 395–406.

Menezes, M.E., Mitra, A., Shevde, L.A., and Samant, R.S. (2012). DNAJB6 governs a novel regulatory loop determining Wnt/β-catenin signalling activity. Biochem. J. *444*, 573–580.

Metz, D.C., and Jensen, R.T. (2008). Gastrointestinal neuroendocrine tumors: pancreatic endocrine tumors. Gastroenterology *135*, 1469–1492.

Midwood, K.S., Valenick, L.V., Hsia, H.C., and Schwarzbauer, J.E. (2004). Coregulation of fibronectin signaling and matrix contraction by tenascin-C and syndecan-4. Mol. Biol. Cell *15*, 5670–5677.

Midwood, K.S., and Orend, G. (2009). The role of tenascin-C in tissue injury and tumorigenesis. J. Cell Commun. Signal *3*, 287–310.

Midwood, K.S., Hussenet, T., Langlois, B., and Orend, G. (2011). Advances in tenascin-C biology. Cell. Mol. Life Sci. *68*, 3175–3199.

Mills, G.B., and Moolenaar, W.H. (2003). The emerging role of lysophosphatidic acid in cancer. Nat. Rev. *3*, 582–591.

Min, J.K., Park, H., Choi, H.J., Kim, Y., Pyun, B.J., Agrawal, V., Song, B.W., Jeon, J., Maeng, Y.S., Rho, S.S., et al. (2011). The WNT antagonist Dickkopf2 promotes angiogenesis in rodent and human endothelial cells. J. Clin. Invest. *121*, 1882–1893.

Minn, A.J., Kang, Y., Serganova, I., Gupta, G.P., Giri, D.D., Doubrovin, M., Ponomarev, V., Gerald, W.L., Blasberg, R., and Massagué, J. (2005). Distinct organ-specific metastatic potential of individual breast cancer cells and primary tumors. J. Clin. Invest. *115*, 44–55.

Miralles, F., Posern, G., Zaromytidou, A.I., and Treisman, R. (2003). Actin dynamics control SRF activity by regulation of its coactivator MAL. Cell *113*, 329–342.

Murphy-Ullrich, J.E., Lightner, V.A., Aukhil, I., Yan, Y.Z., Erickson, H.P., and Höök, M. (1991). Focal adhesion integrity is downregulated by the alternatively spliced domain of human tenascin. J. Cell Biol. *115*, 1127–1136.

Nevins, J.R. (2001). The Rb/E2F pathway and cancer. Hum. Mol. Genet. *10*, 699–703.

Oh, H., Ryu, J.H., Jeon, J., Yang, S., Chun, C.H., Park, H., Kim, H.J., Kim, W.S., Kim, H.H., Kwon, Y.G., and Chun, J.S. (2012). Misexpression of Dickkopf-1 in endothelial cells, but not in chondrocytes or hypertrophic chondrocytes, causes defects in endochondral ossification. J. Bone Miner. Res. *27*, 1335–1344.

Orend, G., Huang, W., Olayioye, M.A., Hynes, N.E., and Chiquet-Ehrismann, R. (2003). Tenascin-C blocks cell-cycle progression of anchorage-dependent fibroblasts on fibronectin through inhibition of syndecan-4. Oncogene *22*, 3917–3926.

Oskarsson, T., Acharyya, S., Zhang, X.H., Vanharanta, S., Tavazoie, S.F., Morris, P.G., Downey, R.J., Manova-Todorova, K., Brogi, E., and Massagué, J. (2011). Breast cancer cells produce tenascin C as a metastatic niche component to colonize the lungs. Nat. Med. *17*, 867–874.

Parangi, S., O'Reilly, M., Christofori, G., Holmgren, L., Grosfeld, J., Folkman, J., and Hanahan, D. (1996). Antiangiogenic therapy of transgenic mice impairs de novo tumor growth. Proc. Natl. Acad. Sci. USA *93*, 2002–2007.

Pendás-Franco, N., Aguilera, O., Pereira, F., González-Sancho, J.M., and Muñoz, A. (2008). Vitamin D and Wnt/beta-catenin pathway in colon cancer: role and regulation of DICKKOPF genes. Anticancer Res. *28*(5A), 2613–2623.

Pipas, J.M., and Levine, A.J. (2001). Role of T antigen interactions with p53 in tumorigenesis. Semin. Cancer Biol. *11*, 23–30.

Reis, M., Czupalla, C.J., Ziegler, N., Devraj, K., Zinke, J., Seidel, S., Heck, R., Thom, S., Macas, J., Bockamp, E., et al. (2012). Endothelial Wnt/β-catenin signaling inhibits glioma angiogenesis and normalizes tumor blood vessels by inducing PDGF-B expression. J. Exp. Med. *209*, 1611–1627.

Ren, S., Johnson, B.G., Kida, Y., Ip, C., Davidson, K.C., Lin, S.L., Kobayashi, A., Lang, R.A., Hadjantonakis, A.K., Moon, R.T., and Duffield, J.S. (2013). LRP-6 is a coreceptor for multiple fibrogenic signaling pathways in pericytes and myofibroblasts that are inhibited by DKK-1. Proc. Natl. Acad. Sci. USA *110*, 1440–1445.

Ruiz, C., Huang, W., Hegi, M.E., Lange, K., Hamou, M.F., Fluri, E., Oakeley, E.J., Chiquet-Ehrismann, R., and Orend, G. (2004). Growth promoting signaling by tenascin-C [corrected]. Cancer Res. *64*, 7377–7385.

Schenk, S., Muser, J., Vollmer, G., and Chiquet-Ehrismann, R. (1995). Tenascin-C in serum: a questionable tumor marker. Int. J. Cancer *61*, 443–449.

Smadja, D.M., d'Audigier, C., Weiswald, L.B., Badoual, C., Dangles-Marie, V., Mauge, L., Evrard, S., Laurendeau, I., Lallemand, F., Germain, S., et al. (2010). The Wnt antagonist Dickkopf-1 increases endothelial progenitor cell angiogenic potential. Arterioscler. Thromb. Vasc. Biol. *30*, 2544–2552.

Song, S., Ewald, A.J., Stallcup, W., Werb, Z., and Bergers, G. (2005). PDGFRbeta+ perivascular progenitor cells in tumours regulate pericyte differentiation and vascular survival. Nat. Cell Biol. *7*, 870–879.

Spencer, J.A., and Misra, R.P. (1999). Expression of the SRF gene occurs through a Ras/Sp/SRF-mediated-mechanism in response to serum growth signals. Oncogene *18*, 7319–7327.

Tanaka, K., Hiraiwa, N., Hashimoto, H., Yamazaki, Y., and Kusakabe, M. (2004). Tenascin-C regulates angiogenesis in tumor through the regulation of vascular endothelial growth factor expression. Int. J. Cancer *108*, 31–40.

Tavazoie, S.F., Alarcón, C., Oskarsson, T., Padua, D., Wang, Q., Bos, P.D., Gerald, W.L., and Massagué, J. (2008). Endogenous human microRNAs that suppress breast cancer metastasis. Nature *451*, 147–152.

van Obberghen-Schilling, E., Tucker, R.T., Saupe, F., Gasser, I., Cseh, B., and Orend, G. (2011). Fibronectin and tenascin-C: accomplices in vascular morphogenesis during development and tumor growth. Int. J. Dev. Biol. *55*, 511–525.

Wenk, M.B., Midwood, K.S., and Schwarzbauer, J.E. (2000). Tenascin-C suppresses Rho activation. J. Cell Biol. *150*, 913–920.

Wu, F.T., Stefanini, M.O., Mac Gabhann, F., and Popel, A.S. (2009). A compartment model of VEGF distribution in humans in the presence of soluble VEGF receptor-1 acting as a ligand trap. PLoS ONE *4*, e5108.

Zhou, A.D., Diao, L.T., Xu, H., Xiao, Z.D., Li, J.H., Zhou, H., and Qu, L.H. (2012). β-Catenin/LEF1 transactivates the microRNA-371-373 cluster that modulates the Wnt/β-catenin-signaling pathway. Oncogene *31*, 2968–2978.

Cell Reports, Volume *5*
Supplemental Information

Tenascin-C Downregulates Wnt Inhibitor Dickkopf-1, Promoting Tumorigenesis in a Neuroendocrine Tumor Model

Falk Saupe, Anja Schwenzer, Yundan Jia, Isabelle Gasser, Caroline Spenle, Benoit Langlois, Martial Kammerer, Olivier Lefebvre, Ruslan Hlushchuk, Tristan Rupp, Marija Marko, Michael van der Heyden, Gerard Cremel, Christiane Arnold, Annick Klein, Patricia Simon-Assmann, Valentin Djonov, Agnes Neuville-Mechine, Irene Esposito, Julia Slotta-Huspenina, Klaus-Peter Janssen, Olivier de Wever, Gerhard Christofori, Thomas Hussenet, and Gertraud Orend

Extended Experimental Procedures

Generation of transgenic RipTNC mice

The human TNC cDNA sequence (GenBank X78565.1) comprising all but AD1 and AD2 extra domains was removed from the HxBL.pBS plasmid (Aukhil et al., 1993) and cloned into the Rip1 expression vector (Hanahan, 1985) for insulin promoter driven expression by using the intermediate pcDNA3.1/Hygro(-) vector (**Figure S1B**). Successful cloning was confirmed by restriction enzyme analysis and partial sequencing. Expression and secretion of TNC was determined in a RT2 cell line by immunostaining and sandwich ELISA. The TNC expression vector was injected into the pronucleus of fertilized oocytes giving rise to transgenic RipTNC mice with stable transmission and expression of the transgene. Transgenic mice were healthy and fertile and did not exhibit any detectable alterations in tissue morphology (**Figure S1F**) nor blood glucose homeostasis (**Figure S1G**). All experimental procedures involving mice were done according to the guidelines of INSERM and the Swiss Federal Veterinary Office.

Generation of tumor mice with different TNC expression levels

RT2 mice (Hanahan, 1985) were bred with RipTNC mice (three lines) or TNCKO mice (Forsberg et al., 1996) to generate RT2/TNC or RT2/TNCKO mice respectively, with different TNC expression levels (**Figure S1D, E**). TNC expression analysis confirmed that tumors of RT2/TNC mice expressed transgenic human TNC (**Figure S1D**), whereas those from RT2/TNCKO mice lacked the TNC protein (**Figure S1E).** Starting at the age of 10

weeks the drinking water was supplemented with 5% (w/v) glucose (FLUKA). Most data were obtained from mice in a C57Bl6 background except results in **Figure 2C, Figure 3C** and **Figure S3C** that were derived from RT2/TNCKO mice and littermates with one TNC copy (RT2/TNC+/-) in a mixed 129/Sv-C57Bl6 background. For genotyping by PCR the following primers were used, RipTNC (Fwd: 5'-TAA TGG GAC AAA CAG CAA AG-3', Rev: 5'-GAA AGA CAC CTG CCA ACA GC-3'), SV40 Tag (Fwd: 5'-GGA CAA ACC ACA ACT AGA ATG CAG-3', Rev: 5'-CAG AGC AGA ATT GTG GAG TGG-3') and TNCKO (Fwd wt: 5'-CTG CCA GGC ATC TTT CTA GC-3', Fwd TNCKO: 5'-CTG CTC TTT ACT GAA GGC TC-3', Rev: 5'-TTC TGC AGG TTG GAG GCA AC-3').

Tumor grading

Tumor grading was performed on H&E stained paraffin sections and classified into adenomas (differentiated tumor cells, encapsulated tumors) and Grade 1 carcinomas (differentiated tumor cells, one invasive tumor front), Grade 2 carcinomas (partially dedifferentiated tumor cells, more than one invasive tumor front) and Grade 3 carcinomas (heterogeneous appearance and loss of differentiated tumor cells, many invasion sites).

Human insulinomas

Tumor material was obtained from the Klinikum rechts der Isar (Munich, Germany) or the Hôpital de Hautepierre (Strasbourg, France) with prior patient informed written consent. Patients underwent surgical resection at the Department of Surgery, Klinikum rechts der Isar, Munich, Germany (between 1991 and 2011) (Group 1) and at the Hôpital de Hautepierre, Strasbourg (between 1994 and 2007) (Group 2). Tissue specimens were transferred into liquid nitrogen and stored until further processing for mRNA extraction, embedded in Tissue-Tek (Sakura, Labonord) and stored at -80°C, or fixed in formalin and embedded in paraffin. The median age of patients from Group 1 was 52 years (35 to 82 years, 5 male and 2 female patients) and of patients from Group 2 was 46 years (13 to 69 years, 2 male and 5 female patients). Presence of metastasis was diagnosed in three

patients (liver or lymph node n = 2, Group 1; liver and lymph node n = 1, Group 2). Analysis by qRTPCR, IF and IHC was performed as described.

Oral glucose tolerance test

12 week old mice (14 RipTNC and 15 wildtype) were starved overnight in clean cages with free access to water. Tail vein blood glucose concentration was measured at time = 0 using Glucofix sensor for Glucofix mio (A. Menarini Diagnostics). 2 mg glucose per g body weight was orally administered by gavage and blood glucose levels (mg/dl) were measured every 15 minutes for 1.5h.

Perfusion, fibrinogen staining and quantification of tumor vessel leakiness

Twelve week old mice were anesthesized by i.p. injection of pentobarbital (5%, 4µl/g body weight). The chest was opened and the right atrium was cut. The left heart ventricle was perfused with 10 ml of 4% paraformaldehyde (PFA) followed by 10 ml of PBS through a 23G syringe connected to a peristaltic pump at constant pressure. The pancreas was dissected, incubated overnight in 20% sucrose at 4°C and frozen in O.C.T. Seven µm sections were processed for fibrinogen and CD31 immunofluorescent staining as described. Fibrinogen immunoreactive areas were measured by using the ImageJ software and were expressed as percentage of tumor/islet total area (area fraction).

Gene expression analysis of mouse tissue and human insulinomas

Tissue from isolated tumors, liver and lung was snap frozen in liquid nitrogen. Total RNA extracted with NucleoSpin RNA II kit (Macherey-Nagel) from liver, KRIB tumors (1 µg), RT2 tumors or lung tissue (2 µg) was treated with DNase I (Invitrogen) and reverse transcribed (MultiScribe reverse transcriptase, Applied Biosystems). qRTPCR was done on cDNA diluted 1:5 (liver, lung) or 1:10 (tumors) with specific primers (Roche Probefinder v2.45, see primer list) on a 7500 Real Time PCR machine (Applied Biosystems) using SYBR green or Taqman reaction mixtures (Applied Biosystems). Data were normalized versus TBP (liver, lung), HMBS (KRIB tumors), GAPDH (human insulinoma) or a combined

value of RPL19, TBP and GAPDH (RT2 tumors). Relative expression levels ($2^{-\Delta\Delta ct}$) were calculated for each individual sample.

Isolation of pancreatic islets

Langerhans islets were isolated from 8 week old RT2 mice by using Liberase RI (Roche) (RT2/TNC and RT2) and Liberase TL (Roche) (RT2/TNCKO and RT2). The pancreas was perfused via the bile duct with 2 ml Liberase solution (0.82 (RI), 1 (TL) Wünsch units/ml), collected and digested at 37°C (24 minutes (Liberase RI), 17 minutes (Liberase TL)). Upon recovery from the interphase of a Histopaque 1077 (Sigma)/DMEM centrifugation gradient (30 minutes, 1500 x g) intact islets were handpicked under a stereomicroscope and quantified as non-angiogenic (white) or angiogenic (red).

Methylmethacrylate (Mercox) casting and SEM analysis

Anaesthetized mice were perfused through the thoracic aorta with a 0.9% sodium chloride/1% heparin/1% procaine solution followed by a freshly prepared Mercox solution (Vilene Japan Hospital Co. Ltd.) containing 0.1 ml accelerator per 5 ml resin. After solidification pancreata were excised and kept for 3 weeks in 7.5% KOH for tissue dissolution. Casts were dehydrated in ethanol and vacuum dried. Samples were mounted on aluminum stubs, sputtered with gold and examined in a Philips XL-30 SFEG scan electron microscope.

Cell culture, gene expression and immunoblotting

Human brain vasculature pericytes (ScienCell 1200), tumor cell lines, monocyte/macrophage cell lines (J774.A1 and RAW264.7) and L cells (fibroblasts, control and overexpression of Wnt-3A) (American Type Culture Collection, Rockville, MD, (ATCC)) were maintained in DMEM/4.5g/l glucose/10% FCS. Cancer associated fibroblasts (CAF) CT5.1 and CT14 were cultured in DMEM/1g/l glucose/10% FCS. BOSC cells (ATCC) were maintained in DMEM/10% FCS supplemented with 1 mM sodium pyruvate/10 mM Hepes and, HUVEC (Promo cell, C-12203) were maintained in

Endothelial cell growth medium (PromoCell, C-22010). T98G:TPM1, T98G:Syndesmos and T98G:shTPM1 cells (Lange et al., 2008; Ruiz et al., 2004) were cultured in DMEM/10%FCS with 400 µg/ml G418.

Human CAFs were isolated from colorectal adenocarcinoma resection specimens from 2 patients that were obtained in accordance with the local ethics committee (Ghent University Hospital) (De Boeck et al., 2013; De Wever et al., 2004). Tissue fragments were cut in 1-2 mm^3 pieces and transferred into a pre-scratched 6-well plate with 100 µl FCS supplemented antibiotica DMEM. Cultures were incubated at 37°C with 10% CO2 in air for 24h. DMEM containing 10% FCS was added into each well. Cell outgrowth was observed after 3-6 days. After 15 days, adherent cells were transferred to 25 cm^2 tissue culture flasks.

Conditioned medium containing Wnt-3A or mDKK1 was collected from L cells overexpressing Wnt-3A and from KRIB cells overexpressing mDKK1, respectively after 3 to 4 days of culture. Medium was filter-sterilized and stored at -20°C. Cells starved in DMEM/1% FCS (tumor cells, pericytes, CAF) or M199/1% FCS/1µg/ml hydrocortison/10 ng/ml heparin/10 ng/ml mEGF/10 ng/ml bFGF (HUVEC) were seeded onto matrix coated dishes as published (Huang et al., 2001; Lange et al., 2007). Briefly, FN and TNC were sequentially coated in PBS/0.01% Tween-20 at 1 µg/cm^2 before saturation of the non-coated surface with 10 mg/ml BSA/PBS.

Cells were starved overnight before treatment with 1, 10 or 30 µM LPA for 3-4h on FN or FN/TNC substrata (Santa Cruz, H_2O), 5 µg/ml Actinomycin D for 30, 60 or 90 minutes (Sigma-Aldrich, DMSO), 5 µg/ml Latrunculin B for 3h (Calbiochem, DMSO) and 2 µg/ml Cytochalasin D four 3h (Calbiochem, DMSO).

Gene expression analysis of cultured cells

RNA was isolated (NucleoSpin RNA extraction kit, Macherey-Nagel or Trizol, Life Technologies) according to the manufacturer's instructions. RNA was reverse transribed (MultiScribe reverse transcriptase, Applied Biosystems) and qRTPCR was done on cDNA diluted 1:2.5 in water with specific primers (see primer list) on a 7500 Real Time PCR

machine (Applied Biosystems) using SYBR green reaction mixture (Applied Biosystems). Data were normalized versus ß2-microglobulin expression and relative expression levels was calculated ($2^{-\Delta\Delta ct}$).

Immunoblotting

For immunoblotting cells were lysed in Laemmli buffer (Laemmli, 1970). Antibodies against the following molecules were used: DKK1 (n-terminal, Sigma-Aldrich, D3195, 1:1500), DKK1 (R&D, AF1096, 1:500), 6x His-tag (Abcam, ab18184, 1:1000), RhoA (Santa-Cruz, sc-418, 1:5000), α-tubulin (CP06, Oncogene, Boston, MA, USA, 1:2000). Secondary antibodies were ECL horseradish peroxidase linked whole anti-rabbit (NA934V) and anti-mouse (NXA931) (GE Healthcare, Buckinghamshire, UK) and donkey anti-goat IgG (sc-2020, Santa Cruz, Biotechnology). Amersham ECL (RPN2106) or Amersham ECL-Plus Western blotting detection system (RPN2132) (GE Healthcare, Buckinghamshire, UK) was used.

Immunofluorescence staining of cultured cells

Cells were fixed in 1% PFA for 10 minutes and permeabilized in PBS-Triton 0.1% for 10 minutes. Cells were stained with anti-vinculin (Abcam; 1/50; 2h) and anti-mouse Alexa-488 (Jackson ImmunoResearch; 1/800; 1h). For phalloidin staining cells were incubated for 20 minutes with phalloidin-tetramethylrhodamine B isothiocyanate (Sigma P1951; 1/200). Nuclei were stained with DAPI (Sigma D9542).

Retrovirus construction and infection, plasmid transfection and reporter assays

For generating mDKK1 cDNA with a V5-His-tag the mDKK1 cDNA (Ruiz et al., 2004) was cloned into the pcDNA3.1-V5-His-TOPO vector (Invitrogen) according to the manufacturer's guidelines. For generating the pQCXIP-mDKK1-V5-His vector a BamHI and an EcoRI site were added in pcDNA3.1-mDKK1-V5-His-TOPO plasmid before the ATG or the stop codon of the mouse DKK1 cDNA respectively, using the GeneEditor™ in vitro

site-directed mutagenesis system, with the primers 5'-GGT GGA ATT GCC CTT GGA TCC ACA TGA TGG TTG TGT-3' and 5'-P-ACC ATC ACC ATT GAG AAT TCA CCC GCT GAT CAG CC-3'. Upon BamHI-EcoRI cleavage, the mDKK1-V5-His fragment was gel purified (NucleoSpin® Extract II, Machery-Nagel, France) and cloned in the BamHI-EcoRI site of the pQCXIP retroviral vector (Clontech, Ozyme, France) generating the pQCXIP-mDKK1-V5-His vector. BOSC cells were transfected with the pQCXIP-mDKK1-V5-His vector or empty control (CTR) vector to obtain retroviruses for transduction of KRIB cells followed by selection with puromycin (2.5 µg/ml). Expression of mDKK1 was determined by qRTPCR and immunoblotting.

T98G were transiently transfected (JetPEI, Polyplus, Strasbourg, France) with plasmids encoding RhoA wt (Addgene Plasmid 12962: pRK5-myc-RhoA-wt), RhoA-Q63L (Addgene Plasmid 12964: pRK5-myc-RhoA-Q63L) and RhoA-T19N (Addgene Plasmid 12963: pRK5-myc-RhoA-T19N). Empty pCB6 plasmid was used for control transfection.

Luciferase reporter assays

For the β-catenin luciferase reporter assay, cells were transiently transfected (JetPEI, Polyplus, Strasbourg, France) with the Super-8xTOPFlash or control Super-8xFOPFlash plasmids (mutant TCF/LEF binding sites) (Veeman et al., 2003) (obtained from Addgene, plasmids 12456 and 12457). Upon seeding for 5h on matrix coated dishes, CM containing Wnt-3A, mDKK1 or CTR medium was added for a total of 48h. TOPFlash luciferase activity was calculated after normalization to Renilla and FOPFlash activity (Dual-luciferase reporter assay system, Promega, Madison, WI, USA).

For SRF luciferase reporter assays T98G cells were transfected with the 3DA.Luc plasmid (provided by Guido Posern, University Halle-Wittenberg, Halle, Germany) encoding c-fos derived SRF binding sites and a pRL-TK plasmid for normalization of the luciferase signal.

A 3177 bp human DKK1 promoter sequence was cloned from HCT116 genomic DNA into

the multiple cloning site of the pGL3-basic luciferase reporter vector (Promega). Cells were transiently transfected with the pGL3-DKK1 promoter construct or empty pGL3-basic vector for 40h. Luciferase activity normalized to Renilla activity is presented as the ratio of pGL3-DKK1 to pGL3-basic.

Generation of KRIB shDKK1 cells

For generation of KRIB shDKK1 cells, KRIB cells were infected with MISSION lentiviral transduction particles (SHCLNV, clone ID TRCN0000033386, Sigmal-Aldrich) or MISSION non-target shRNA control transduction particles (SHC002V, Sigma-Aldrich) with a MOI = 10 and, transduced cells were selected with 10 µg/ml puromycin.

Cell proliferation assay

To determine cell proliferation, cells were plated into 96-well plates (5 x 10^3 cells/well in quadruplicate for each time point). A MTS assay was performed following manufacturer's instructions (CellTiter 96® aqueous non-radioactive cell proliferation assay, Promega) after 24h (day 1), 48h (day 2) and 72h (day 3). Measures were normalized to the relative cell number on day 1.

HUVEC tubulogenesis assay

Tubulogenesis assessment was done in 15 well dishes (µ-Slide Angiogenesis, Ibidi LLC), using growth factor reduced Matrigel (BD Bioscience). The matrix was prepared by loading 10 µl of Matrigel in each well followed by solidification for 45-60 minutes at 37°C in a humidified incubator. HUVEC (Promocell) were trypsinized and resuspended at 100,000 cell/ml in conditioned medium (CM) obtained from KRIB cells overexpressing mouse DKK1 or its respective control (CM was collected after 2 days in confluent layers of both KRIB cell types). 5 X 10^3 cells/well (50 µl) were loaded on top of the solidified Matrigel and was incubated for 6h at 37°C in a humidified incubator in a 5% CO2 atmosphere. Bright field mosaic pictures were taken using a Zeiss Imager Z2 inverted microscope and AxioVision software (Carl Zeiss) at 5X magnification, which allowed

imaging of the whole well in 9 pictures. Tube-like structures (defined by the numbers of closed loops) were counted using the ZEN Blue software (Carl Zeiss). 3 independent experiments were performed with 3-5 replicates per experiment, and measures subsequently were averaged.

Tumor xenograft experiments

4 x 10^6 KRIB CTR or mDKK1 overexpressing cells were injected subcutaneously in the left upper back of nude mice (Charles River). After 3.5 weeks, mice were sacrificed, the tumor size was measured with a caliper and the tumor volume was calculated using formula $V=(a^2*b)/2$, where b is the longest axis and a is the perpendicular axis to b. Tumor tissue was snap frozen in liquid nitrogen or directly embedded in O.C.T. and further analyzed by qRTPCR and immunostaining as described.

VEGFA/TNC binding study

Surface plasmon resonance binding experiments were performed on a Biacore 2000 instrument (Biacore Inc.) at 25°C. VEGFA165 (Millipore) or TNC (Huang et al., 2001) were immobilized at high surface density (around 7000 resonance units) on an activated CM5 chip (Biacore Inc.) using a standard amine-coupling procedure according to the manufacturer's instruction. Soluble molecules were added at a concentration of 10 µg/ml in 10 mm sodium acetate, pH 5.0, and at a flow rate of 5 µl/min for 20 min before addition of 1 M ethanolamine. Soluble TNC (5 - 20µg in 200µl) or VEGFA165 was added to the chip in 10 mm MES, pH 6.0, 150 mm sodium chloride, 0.005% (v/v) surfactant P20, at a flow rate of 10 µl/min. A blank CM5 chip was used for background correction. 10 mm glycine, pH 2.0, at 100 µl/min for 1 min was used to regenerate the chip surface between two binding experiments. A steady state condition was used to determine the affinity of VEGFA165 for TNC and the affinity of TNC for VEGFA165. The Dissociation constant (Kd) was determined using the 1:1 Langmuir association model as described by the manufacturer.

Statistical analysis and graphical representation

Statistical analysis was performed using GraphPad Prism. For significance of an association (contingency) Fisher's exact test was applied (tumor staging, gene expression, metastasis incidence). Statistical differences were analyzed by unpaired t-test (Gaussian distribution) or nonparametric Mann-Whitney test (no Gaussian distribution). Gaussian data sets with different variances were analyzed by unpaired t-test with Welch's correction. Gaussian distribution was tested by the Shapiro-Wilk normality test. p-values < 0.05 were considered as statistically significant.

Primer list for qRTPCR on tumor, liver and lung tissue

Gene	Species	Forward primer	Reverse primer
Axin2	mouse	CTGCTGGTCAGGCAGGAG	TGCCAGTTTCTTTGGCTCTT
CD44	mouse	GTCTGCATCGCGGTCAATAG	GGTCTCTGATGGTTCCTTGTTC
CyclinD1	mouse	CGCACTTTCTTTCCAGAGTCA	AAGGGCTTCAATCTGTTCCTG
DKK1	mouse	Taqman (ABI) Mm00438422_m1	
DKK1	mouse	CCGGGAACTACTGCAAAAAT	CCAAGGTTTTCAATGATGCTT
DKK2	mouse	GCCAAACTCAACTCCATCAAG	TCACTGCTGCAAGGGTAGG
Dll4	mouse	AGGTGCCACTTCGGTTACAC	GGGAGAGCAAATGGCTGATA
E-Cadherin	mouse	CAGCCTTCTTTTCGGAAGACT	GGTAGACAGCTCCCTATGACTG
GAPDH	mouse	Taqman (ABI) Mm99999915_g1	
GAPDH	human	ATCTTCTTTTGCGTCGCCAG	AATCCGTTGACTCCGACCTTC
Hey-1	mouse	CATGAAGAGAGCTCACCCAGA	TTGGGGACATGGAACACAG
HMBS	human	Qiagen QT00494130 (for Sybr green)	
Insulin	mouse	TGGCTTCTTCTACACACCCAAG	ACAATGCCACGCTTCTGCC
Insulin	mouse	Taqman mIns1 Mm01259683_g1	
Lgr5	mouse	GGAAAGAAATGCTTTGATGGAC	AGTGGGGAATTCATCAAGGTT
RPL19	mouse	ACCCTGGCCCGACGG	TACCCTTCCTCTTCCCTATGCC
Slug	mouse	GAAAAGCACATTGCATCTTTTCT	TGTTCCTTTGGTTGAAATGGT
TBP	mouse	CCCCACAACTCTTCCATTCT	GCAGGAGTGATAGGGGTCAT
TNC	human	GTCACCGTGTCAACCTGATG	GTTAACGCCCTGACTGTGGT

Primer list for qRTPCR on cultured cells

Gene	Forward primer	Reverse primer
Axin2	CCACACCCTTCTCCAATCC	TGCCAGTTTCTTTGGCTCTT
DKK-1	GACCATTGACAACTACCAGCCG	TACTCATCAGTGCCGCACTCCT
DKK-2	GGCAGTAAGAAGGGCAAAAA	CCTCCCAACTTCACACTCCT

DKK-3	GAGGACACGCAGCACAAA	TGCCAGGTTCACTTCTGATG
DKK-4	AGGAGGTGCCAGCGAGAT	CATCTTCCATCGTAGTACAAACATC
SFRP1	GCTGGAGCACGAGACCAT	TGGCAGTTCTTGTTGAGCA
SFRP2	GCTTGAGTGCGACCGTTT	CAGGCTTCACATACCTTTGGA
SFRP3/FRZB	GGGCTATGAAGATGAGGAACG	CTGAGTCCAAGATGACGAAGC
SFRP4	CGATCGGTGCAAGTGTAAAA	ACCACCGTTGTGACCTCATT
SRF	AGACGGGCATCATGAAGAAG	TGATCATGGGCTGCAGTTT
TPM1	CCCGTAAGCTGGTCATCATC	CTTGTGTGCTCATCATTCCGA
RhoA [1](Sauzeau et al., 2003)	GCAGGTAGAGTTGGCTTTATGG	CTTGTGTGCTCATCATTCCGA
β2-Microglobulin	GTGGGATCGAGACATGTAAGCA	AATGCGGCATCTTCAAACCT

[1], Sauzeau et al., 2003

Table S1 Carcinoma progression by TNC - Related to Figure 1

Genotype	Adenomas (%)	Carcinomas (%)				
		Grade 1	Grade 2	Grade 3	Grade 1 - 3	Ca/Ad
RT2	55.8	32.7	10.5	0.9	44.2	0.8
RT2/TNC	35.7	39.9	21.3	3.2	64.3	1.8

Numbers of adenomas and carcinomas Grade 1 to 3 in 12 week old mice. Average frequency of each tumor grade per mouse is displayed; 26 RT2 mice (78 adenomas, 79 carcinomas) and 22 RT2/TNC mice (44 adenomas, 76 carcinomas). p = 0.038, Fisher's exact test. RT2/TNC mice developed 1.8-fold more carcinomas than adenomas (p = 0.001, Student's t-test) compared to RT2 mice (0.8-fold, p = 0.945, Student's t-test).

Table S2 TNC dependent angiogenic switch - Related to Figure 1

Genotype	All islets			Islets per mouse	
	A plus NA	A	NA	A	NA
RT2 (n = 9)	826	71	755	7.9 (±2.2)	83.9 (±7.4)
RT2/TNC (n = 7)	810	136	674	19.4 (±4.3)	96.3 (±10.0)
RT2/TNC versus RT2 (fold)				2.46	1.15
p-value		< 0.0001 [a]		0.0226 [b]	0.3248 [b]
RT2 (n = 7)	809	255	554	36.4 (±5.0)	79.1 (±8.6)
RT2/TNCKO (n = 7)	840	87	753	12.4 (±2.6)	107.6 (±11.8)
RT2/TNCKO versus RT2 (fold)				- 2.94	1.36
p-value		< 0.0001 [a]		0.0011 [c]	0.2008 [b]

Angiogenic (A) and non-angiogenic (NA) islets were isolated from 8 week old RT2 mice with the indicated genotypes and were quantified (average number including SEM per mouse). Islets from RT2 littermates were prepared independently in both series of experiments. (a) Fisher's exact test, (b) Student's t-test, (c) Mann Whitney test. Note that differences between RT2 controls originate from inherent experimental conditions (e.g. efficiency of collagenase treatment).

Table S3 Gene expression analysis of RT2 and RT2/TNC tumors - Related to Figure 3

Gene	Tumor class	Relative expression	p-value	Gene	Tumor class	Relative expression	p-value
Axin2	All	**1.35**	0.008	**Dll4**	All	1.66	0.153
	Small	**1.30**	0.034		Small	1.55	0.186
	Small+Diff	1.27	0.055		Small+Diff	1.43	0.258
	Big	1.49	0.194		Big	1.93	0.376
	Big+Diff	1.18	0.571		Big+Diff	1.61	0.786
	Diff	**1.25**	0.037		Diff	1.45	0.194
CD44	All	1.64	0.225	**Hey-1**	All	-1.27	0.134
	Small	1.72	0.077		Small	-1.02	0.911
	Small+Diff	**2.06**	0.029		Small+Diff	1.03	0.843
	Big	-1.63	0.133		Big	**-3.08**	0.019
	Big+Diff	-1.58	0.143		Big+Diff	**-2.67**	0.036
	Diff	1.85	0.157		Diff	-1.16	0.343
CyclinD1	All	1.45	0.166	**Lgr5**	All	-6.81	0.931
	Small	1.45	0.113		Small	-1.72	0.477
	Small+Diff	**2.01**	0.037		Small+Diff	-1.73	0.340
	Big	1.17	0.776		Big	-23.06	0.279
	Big+Diff	-1.02	0.571		Big+Diff	-6.74	0.786
	Diff	1.78	0.112		Diff	-2.65	0.528
DKK1	All	**-16.07**	0.035	**Slug**	All	1.28	0.220
	Small	-16.34	0.062		Small	**1.67**	0.010
	Small+Diff	**-4.13**	0.043		Small+Diff	**1.84**	0.004
	Big	-15.49	n.a.		Big	-2.56	0.081
	Big+Diff	-3.19	n.a.		Big+Diff	-2.20	0.294
	Diff	**-3.90**	0.044		Diff	1.46	0.063
DKK2	All	-1.85	0.204				
	Small	-1.46	0.551				
	Small+Diff	-1.35	0.841				
	Big	**-3.69**	0.032				
	Big+Diff	**-4.67**	0.036				
	Diff	-1.85	0.366				

Relative gene expression in RT2/TNC versus RT2 tumors as determined by qRTPCR. RNA was isolated from tumors of 14 week old RT2 (N = 11 mice, n = 27 tumors) and RT2/TNC mice (N = 3, n = 13). Data are presented for all tumors (All) and subgroups : small tumors (Small : 1 – 3 mm in diameter, RT2 (n = 19), RT2/TNC (n = 10)), big

tumors (Big : > 3 mm, RT2 (n = 8), RT2/TNC (n = 3)), differentiated tumors (Diff. : high expression of insulin and E-cadherin, RT2 (n = 22), RT2/TNC (n = 13)), small and differentiated tumors (Small + Diff : RT2 (n = 17), RT2/TNC (n = 10)) and big and differentiated tumors (Big + Diff, RT2 (n = 5), RT2/TNC (n = 3)). Bold numbers represent statistically significant changes in relative expression, n.a., not applicable due to low sample number.

Fig. S1

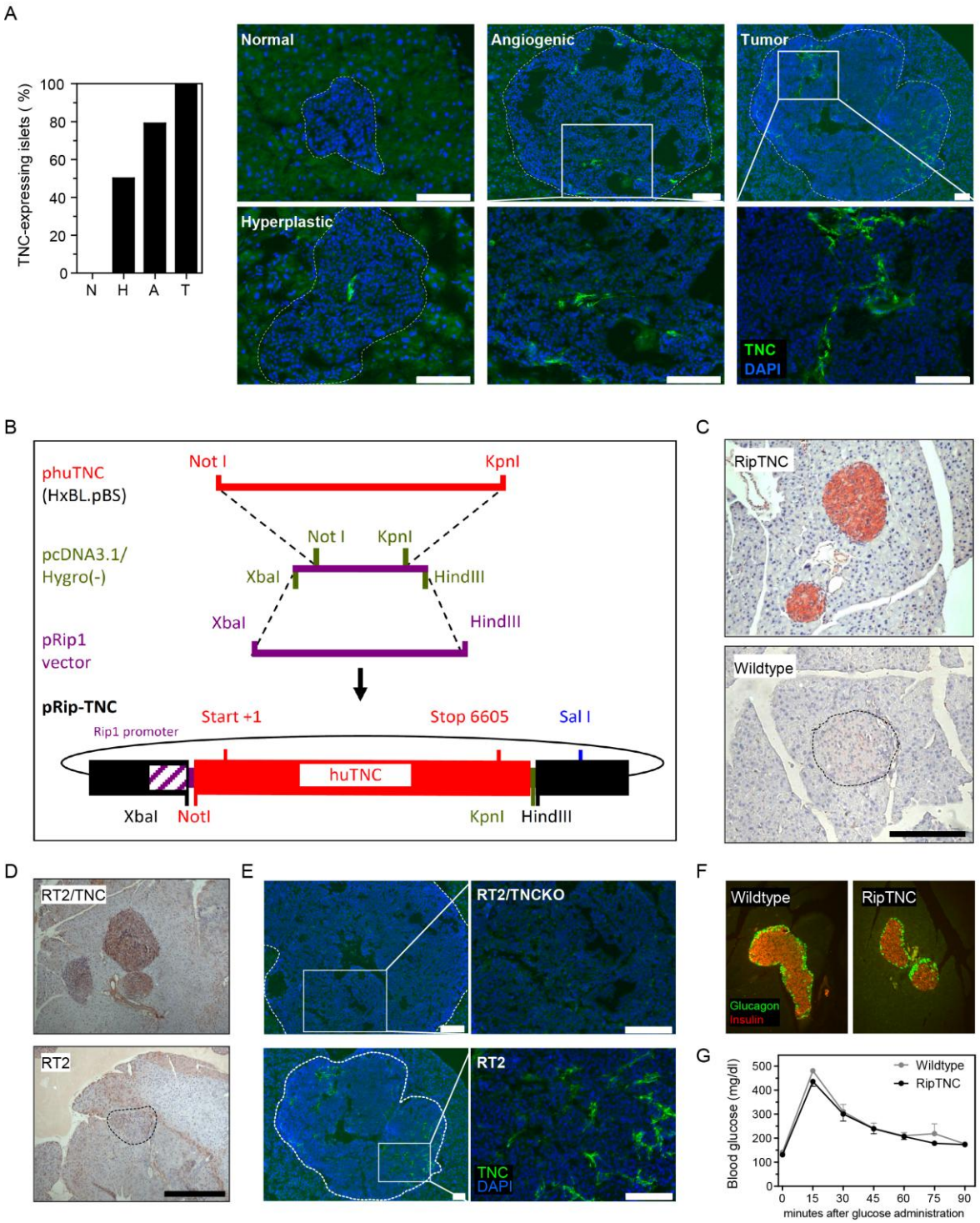

Figure S1 TNC expression in RT2 mice, TNC expression vector and impact of transgenic TNC on pancreatic tissue function. Related to Figure 1

(A) TNC expression in RT2 islets determined by IF analysis (MTn12 antibody) in tissue sections of 12 week old RT2 mice. In contrast to the absence of TNC from normal islets (N < 0.2 mm diameter), TNC is expressed in 50%, 80% and 100% of hyperplastic (H, 0.2 – 0.5 mm diameter), angiogenic (A, > 0.5 – 1 mm diameter) and tumorigenic islets

(T, diameter above 1 mm), respectively. Right panels, dotted lines delineate the islet circumferences. 82 islets (N = 26, H = 34, A = 14, T = 8) of 3 RT2 mice were analyzed. Scale bar, 100 μm. **(B)** Strategy for the generation of the TNC expression vector. The human cDNA (Gherzi et al., 1995) was removed from the HxBL-pBS plasmid (Aukhil et al., 1993) and cloned into the Rip1 expression vector (Hanahan, 1985) for insulin-promoter driven expression of the transgene by using the pcDNA3.1./Hygro(-) plasmid as intermediate vector. The inserted human cDNA sequence comprises 45 nucleotides upstream of the start site and 639 nucleotides downstream of the stop signal. **(C-E)** TNC expression analysis in RipTNC **(C),** RT2/TNC **(D)** and RT2/TNCKO pancreatic tissue **(E)** by IHC **(C, D)**, IF **(E)**. Scale bar 100 μm. **(F)** No sorting difference of α-glucagon and insulin positive α- and β-cells in pancreatic tissue of wildtype and RipTNC mice was observed as determined by IF. **(G)** Determination of blood glucose levels after an oral glucose tolerance test in 14 RipTNC and 15 wildtype mice. Average ±SEM is presented for each time point.

Fig. S2

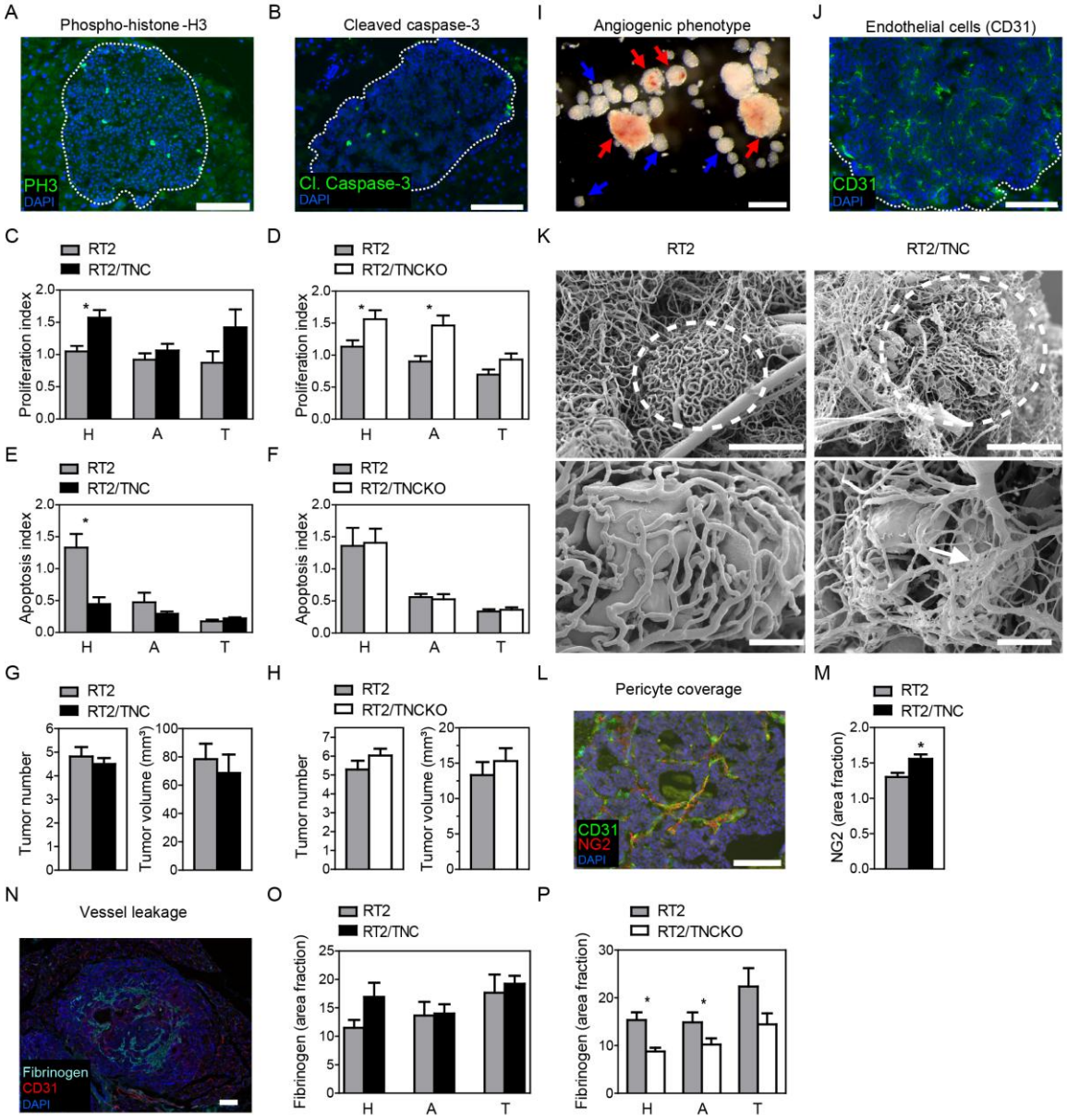

Figure S2. Expression analysis, islet quantification, tumor incidence and burden, Related to Figure 1

(A, B, J, L, N) Expression of the indicated molecules in RT2 tumor tissue upon IF analysis. Scale bar 100 µm. **(C, D)** Quantification of proliferation according to tumor stage in 12 week old mice, **(C)** RT2, 9 mice, 99 hyperplastic (H), 37 angiogenic (A) and 14 tumorigenic (T) islets; RT2/TNC, 8 mice, H = 71, A = 47, T = 22, **(D)** RT2, 6 mice, H = 73, A = 38, T = 20; RT2/TNCKO, 6 mice, H = 72, A = 40, T = 25. **(C)** In RT2/TNC mice a significant 1.5 - fold increase in proliferation in hyperplastic islets is observed. **(D)** a signifcant increase in proliferation in hyperplastic (1.4-fold) and angiogenic (1.6-fold) islets from RT2/TNCKO mice is observed. **(E, F)** Quantification of apoptosis in 12 week

old mice, **(E)** RT2, 6 mice, H = 55, A = 19, T = 10; RT2/TNC, 8 mice, H = 59, A = 43, T = 21, **(F)** RT2, 4 mice, H = 56, A = 26, T = 13; RT2/TNCKO, 4 mice, H = 72, A = 40, T = 25. In hyperplastic islets of RT2/TNC mice a significant 2.9-fold decrease in apoptosis is observed, while no significant difference was seen in RT2/TNCKO mice. **(G, H)** Tumor incidence and burden, **(G)** RT2, N = 33 mice, RT2/TNC, N = 26, **(H)** RT2, N = 28, RT2/TNCKO, N = 31. Differences were not statistically significant. **(I)** Image of isolated angiogenic and non-angiogenic islets of an 8 week old RT2 mouse. Scale bar 500 µm. Red arrows: angiogenic islets, blue arrows: non-angiogenic islets. **(K)** Representative SEM pictures from RT2 (N = 5 mice) and RT2/TNC tumors (N = 3). Arrow points at small aggregated vessels. Scale bars: top panels 200 µm, bottom panels 100 µm. **(M)** Quantification of NG2, a marker for pericytes, area fraction in 12 week old RT2 (N = 6 mice, n = 155 islets) and RT2/TNC (N = 8 mice, n = 204 islets) mice. A significant 1.2-fold increase of NG2 area fraction is observed in RT2/TNC islets. **(O, P)** Quantification of fibrinogen, a marker of vessel leakiness; area fraction according to tumor stage in 12 week old mice, **(O)** RT2, 5 mice, H = 36, A = 18, T = 8; RT2/TNC, 3 mice, H = 26, A = 20, T = 4; **(P)** RT2, 4 mice, H = 35, A = 18, T = 7; RT2/TNCKO, 5 mice, H = 59, A = 47, T = 9. **(O)** In hyperplastic islets of RT2/TNC mice an increased fibrinogen leakiness is observed (1.5-fold, p = 0.06). **(P)** In hyperplastic (1.8-fold) and angiogenic islets (1.5-fold) of RT2/TNCKO mice, a significant decrease of fibrinogen area fraction is observed. Error bars represent SEM and asterisks (*) indicate p values < 0.05.

Fig. S3

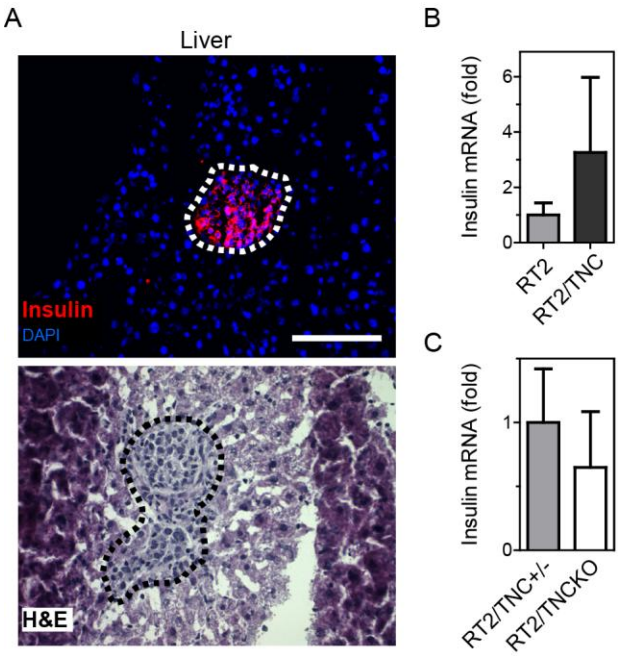

Figure S3. Liver micrometastasis in RT2 mice, Related to Figure 2

(A) Detection of insulin expressing tumor cells in liver tissue of a RT2 mouse by IF (upper panel) and H&E of a neighboring section (lower panel). Scale bar, 50 μm. **(B, C)** Quantification of insulin expression in liver tissue of RT2 mice. Insulin expression was detected in RT2/TNC (7/24) and RT2 (6/24) **(B)** and RT2/TNCKO (5/10) and RT2/TNC+/- littermates (6/8) **(C)**. Differences were not statistically significant. Error bars represent SEM.

Fig. S4

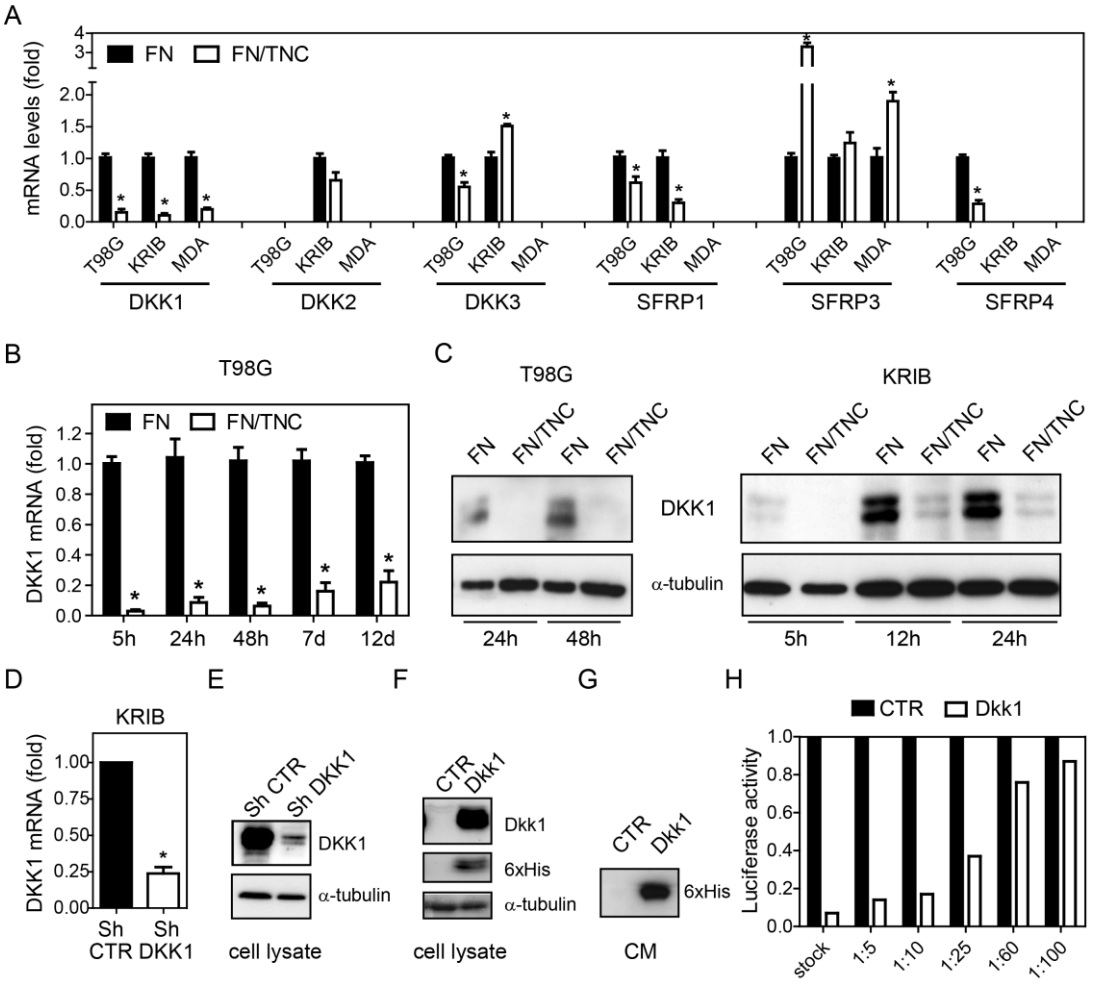

Figure S4. Impact of TNC on the expression of Wnt inhibitors, DKK1 downregulation and activation of Wnt signaling in tumor cells, Related to Figure 4

(A) Expression of Wnt inhibitors in T98G, KRIB and MDAMB-435 (MDA) cells as determined by qRTPCR upon plating on the indicated substrata for 24h (KRIB, MDAMB-435) or 48h (T98G). There was no expression of SFRP2 nor DKK4 detectable in any of the cell lines and conditions tested. **(B)** DKK1 expression (qRTPCR) upon plating T98G cells on FN/TNC and FN for the indicated time. DKK1 expression on FN/TNC is represented relative to its expression on FN. **(C)** Reduced DKK1 protein levels by TNC in T98G or KRIB cells upon plating for the indicated time as determined by immunoblotting. **(D, E)** Reduced DKK1 expression upon shRNA mediated DKK1 knockdown as determined by qRTPCR **(D)** and immunoblotting **(E)** in KRIB Sh-DKK1 cells in comparison to KRIB Sh-control (CTR) cells. **(F)** Expression of murine DKK1 in control (CTR) and mDKK1

overexpressing KRIB cells. Overexpression of murine DKK1 in KRIB:mDKK1 cells. Lysates of KRIB cells expressing His-tagged mDKK1 or empty vector control were analyzed by immunoblotting with antibodies against DKK1 or the His-tag. **(G)** Expression of murine DKK1 in the conditioned media (CM) from control (CTR) and mDKK1 overexpressing KRIB cells. Supernatants from the KRIB cells expressing His-tagged mDKK1 or empty vector control were analyzed by immunoblotting. **(H)** Addition of DKK1 containing CM assessed by immunoblotting inhibits TOPFlash activity in KRIB cells in a dose dependent manner. KRIB cells were plated for 48h and treated with increasing dilutions of CM from KRIB:mDKK1 cells. Data are derived from at least 3 independent experiments, except for (**H**). Error bars represent SEM and asterisks (*) indicate p values < 0.05.

Fig. S5

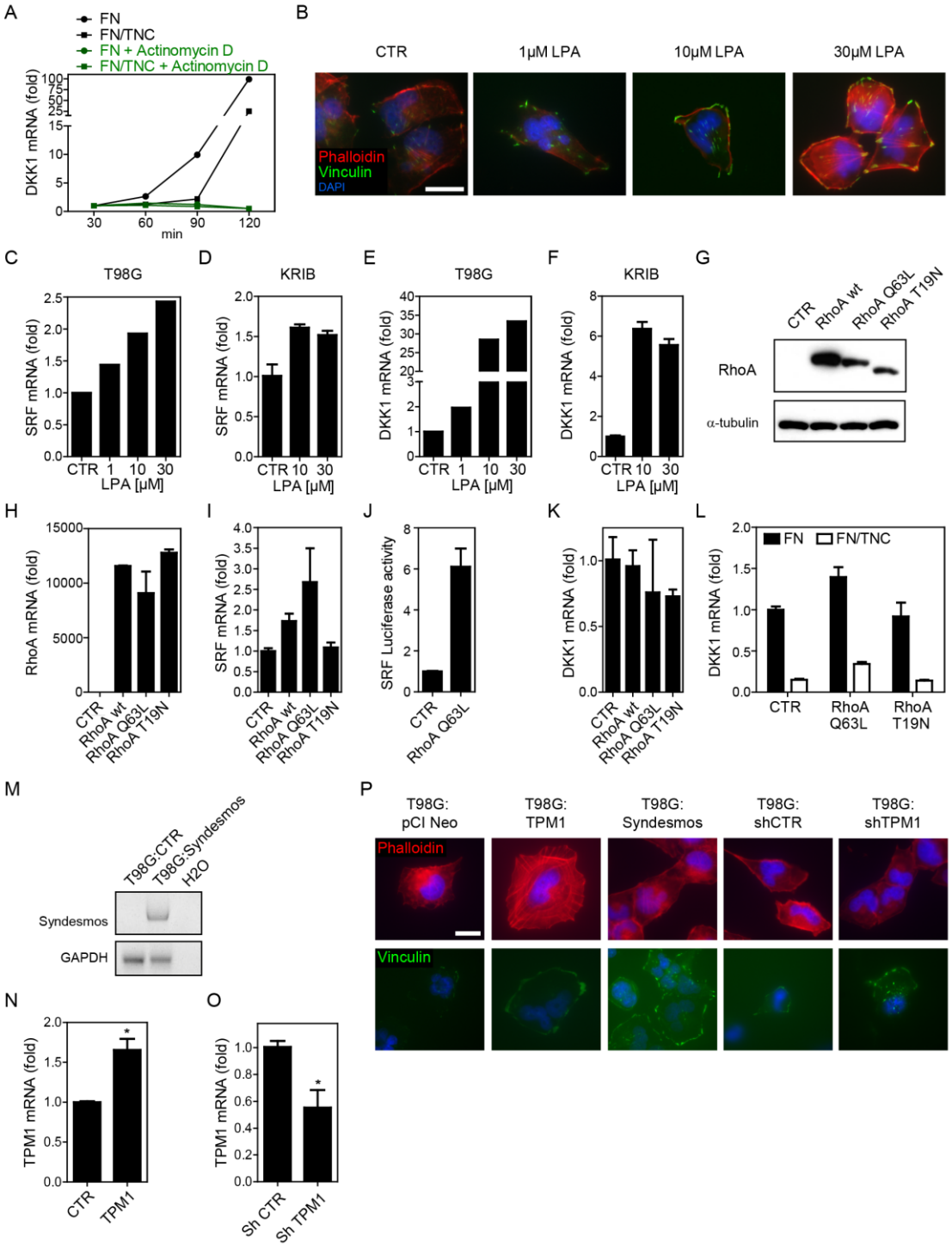

Figure S5. Mechansim of DKK1 downregulation, Related to Figure 5

(A) Serum starved T98G cells were seeded on FN or FN/TNC. After 30 minutes 5 μg/ml Actinomycin D was added and cells were lysed after an additional 30, 60 or 90 minutes for analysis of DKK1 mRNA expression. **(B)** Serum starved T98G cells were treated with the indicated concentrations of LPA. IF staining of vinculin (green) and phalloidin (red). **(C, D)** SRF and **(E, F)** DKK1 mRNA expression of serum starved T98G and KRIB cells

treated with the indicated concentrations of LPA. **(G-L)** T98G cells were transfected with RhoA wt, RhoA Q63L (CA) or RhoA T19N (DN). **(G, H)** Overexpression of RhoA was validated by immunoblotting **(G)** and qRTPCR **(H). (I, J)** SRF mRNA expression **(I)** and SRF luciferase activity of T98G cells **(J). (K, L)** DKK1 mRNA expression analysed by qRTPCR of cells seeded on uncoated **(K)** or FN and FN/TNC coated dishes **(L). (M)** RTPCR for chicken syndesmos of T98G CTR and T98G:syndesmos cells. **(N, O)** TPM1 mRNA levels analyzed by qRTPCR in T98G:TPM1 **(N),** T98G:shTPM1 **(O)** and control cells. **(P)** IF of vinculin (green) and phalloidin (red) in T98G control, T98G:TPM1, T98G:syndesmos and T98G:shTPM1 cells. Nuclei are stained with DAPI (blue). Error bars represent SEM and asterisks (*) indicate p values < 0.05.

Fig. S6

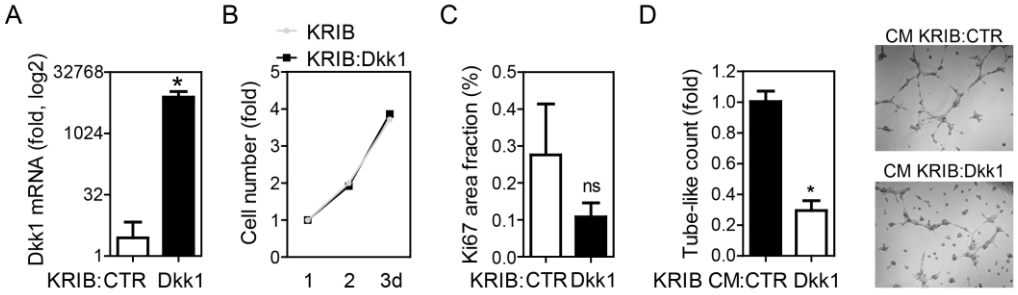

Figure S6. DKK1 expression in KRIB:mDKK1 tumors and impact of DKK1 overexpression on tumor cell proliferation and migration, Related to Figure 6

(A) Quantification of murine *Dkk1* gene expression by qRTPCR in control or Dkk1 overexpressing KRIB derived tumors. **(B)** Dkk1 does not change tumor cell proliferation *in vitro*. Proliferation of KRIB (parental) and KRIB:Dkk1 cells was analyzed with a MTS assay. Data are normalized in each group to values of day 1. **(C)** Dkk1 does not change tumor cell proliferation *in vivo*. Proliferating cells were quantified in tumors derived from KRIB control or KRIB:Dkk1 cells. Ki67-positive areas were determined using ImageJ software upon staining for Ki67 and reported to the DAPI positive areas per tumor. No significant (ns) difference was observed (n = 5 per group). **(D)** HUVEC tubulogenesis on Matrigel upon addition of CM derived from KRIB control or Dkk1 overexpressing cells. Quantification of three independent experiments (left) and representative phase contrast pictures (right) are shown. Error bars represent SEM and asterisks (*) indicate p values < 0.05.

Fig. S7

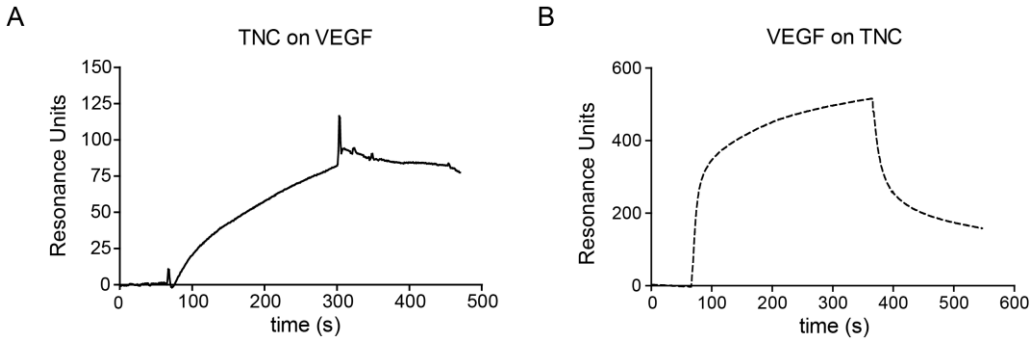

Figure S7. Binding of TNC to VEGFA

Binding of VEGFA to TNC was determined by Biacore including normalization to a blank surface. Binding of TNC and VEGFA to a sensorchip adsorbed with VEGFA **(A)** and TNC **(B)**, respectively is shown. We observed that VEGFA and TNC bind to each other in a dose dependent manner with a Kd of 2.7 x 10^{-7} M (TNC binding to VEGFA) and 1.5 x 10^{-9} M (VEGFA binding to TNC) which is lower than VEGFA binding to its receptor (3.3 x 10^{-11} M) but is in the range of a VEGFA/glycosaminogycan interaction (2.4 x 10^{-8} M) (Wu et al., 2009).

References to SI Material

Aukhil, I., Joshi, P., Yan, Y., and Erickson, H.P. (1993). Cell- and heparin-binding domains of the hexabrachion arm identified by tenascin expression proteins. J Biol Chem *268*, 2542-2553.

De Boeck, A., Hendrix, A., Maynard, D., Van Bockstal, M., Daniels, A., Pauwels, P., Gespach, C., Bracke, M., and De Wever, O. (2013). Differential secretome analysis of cancer-associated fibroblasts and bone marrow-derived precursors to identify microenvironmental regulators of colon cancer progression. Proteomics *13*, 379-388.

De Wever, O., Nguyen, Q.D., Van Hoorde, L., Bracke, M., Bruyneel, E., Gespach, C., and Mareel, M. (2004). Tenascin-C and SF/HGF produced by myofibroblasts in vitro provide convergent pro-invasive signals to human colon cancer cells through RhoA and Rac. Faseb J *18*, 1016-1018.

Forsberg, E., Hirsch, E., Frohlich, L., Meyer, M., Ekblom, P., Aszodi, A., Werner, S., and Fassler, R. (1996). Skin wounds and severed nerves heal normally in mice lacking tenascin-C. Proceedings of the National Academy of Sciences of the United States of America *93*, 6594-6599.

Gherzi, R., Ponassi, M., Gaggero, B., and Zardi, L. (1995). The first untranslated exon of the human tenascin-C gene plays a regulatory role in gene transcription. FEBS letters *369*, 335-339.

Hanahan, D. (1985). Heritable formation of pancreatic beta-cell tumours in transgenic mice expressing recombinant insulin/simian virus 40 oncogenes. Nature *315*, 115-122.

Huang, W., Chiquet-Ehrismann, R., Moyano, J.V., Garcia-Pardo, A., and Orend, G. (2001). Interference of tenascin-C with syndecan-4 binding to fibronectin blocks cell adhesion and stimulates tumor cell proliferation. Cancer research *61*, 8586-8594.

Laemmli, U.K. (1970). Cleavage of structural proteins during the assembly of the head of bacteriophage T4. Nature *227*, 680-685.

Lange, K., Kammerer, M., Hegi, M.E., Grotegut, S., Dittmann, A., Huang, W., Fluri, E., Yip, G.W., Gotte, M., Ruiz, C.*, et al.* (2007). Endothelin receptor type B counteracts tenascin-C-induced endothelin receptor type A-dependent focal adhesion and actin stress fiber disorganization. Cancer research *67*, 6163-6173.

Lange, K., Kammerer, M., Saupe, F., Hegi, M.E., Grotegut, S., Fluri, E., and Orend, G. (2008). Combined lysophosphatidic acid/platelet-derived growth factor signaling triggers glioma cell migration in a tenascin-C microenvironment. Cancer research *68*, 6942-6952.

Ruiz, C., Huang, W., Hegi, M.E., Lange, K., Hamou, M.F., Fluri, E., Oakeley, E.J., Chiquet-Ehrismann, R., and Orend, G. (2004). Growth promoting signaling by tenascin-C Cancer research *64*, 7377-7385.

Sauzeau, V., Rolli-Derkinderen, M., Marionneau, C., Loirand, G., and Pacaud, P. (2003). RhoA expression is controlled by nitric oxide through cGMP-dependent protein kinase activation. J Biol Chem *278*, 9472-9480.

Veeman, M.T., Slusarski, D.C., Kaykas, A., Louie, S.H., and Moon, R.T. (2003). Zebrafish prickle, a modulator of noncanonical Wnt/Fz signaling, regulates gastrulation movements. Curr Biol *13*, 680-685.

Wu, F.T., Stefanini, M.O., Mac Gabhann, F., and Popel, A.S. (2009). A compartment model of VEGF distribution in humans in the presence of soluble VEGF receptor-1 acting as a ligand trap. PloS one *4*, e5108.